MARTIN MARIETTA ENERGY SYSTEMS LIBRARIES

3 4456 0285622 9

ORNL/TM-5602

Cy 1

Development of a Fissile Particle for HTGR Fuel Recycle

F. J. Homan
E. L. Long, Jr.
T. B. Lindemer
R. L. Beatty
T. N. Tiegs

OAK RIDGE NATIONAL LABORATORY
CENTRAL RESEARCH LIBRARY
DOCUMENT COLLECTION
LIBRARY LOAN COPY
DO NOT TRANSFER TO ANOTHER PERSON
If you wish someone else to see this
document, send in name with document
and the library will arrange a loan.

UCN-7969
(3 3-67)

OAK RIDGE NATIONAL LABORATORY
OPERATED BY UNION CARBIDE CORPORATION FOR THE ENERGY RESEARCH AND DEVELOPMENT ADMINISTRATION

Printed in the United States of America. Available from
National Technical Information Service
U.S. Department of Commerce
5285 Port Royal Road, Springfield, Virginia 22161
Price: Printed Copy $4.50; Microfiche $3.00

This report was prepared as an account of work sponsored by the United States Government. Neither the United States nor the Energy Research and Development Administration/United States Nuclear Regulatory Commission, nor any of their employees, nor any of their contractors, subcontractors, or their employees, makes any warranty, express or implied, or assumes any legal liability or responsibility for the accuracy, completeness or usefulness of any information, apparatus, product or process disclosed, or represents that its use would not infringe privately owned rights.

ORNL/TM-5602
Distribution
Category UC-77

Contract No. W-7405-eng-26
METALS AND CERAMICS DIVISION

HTGR BASE TECHNOLOGY PROGRAM
Fueled Graphite Development (189a OH002)

DEVELOPMENT OF A FISSILE PARTICLE FOR HTGR FUEL RECYCLE

F. J. Homan, E. L. Long, Jr., T. B. Lindemer,
R. L. Beatty, and T. N. Tiegs

Date Published: December 1976

NOTICE This document contains information of a preliminary nature. It is subject to revision or correction and therefore does not represent a final report.

OAK RIDGE NATIONAL LABORATORY
Oak Ridge, Tennessee 37830
operated by
UNION CARBIDE CORPORATION
for the
ENERGY RESEARCH AND DEVELOPMENT ADMINISTRATION

MARTIN MARIETTA ENERGY SYSTEMS LIBRARIES

3 4456 0285622 9

CONTENTS

ABSTRACT 1

INTRODUCTION 1

EARLY WORK WITH OXIDE SYSTEMS AND PERFORMANCE LIMITATIONS OF OXIDE FUELS 2

PROCESSING CONSIDERATIONS 6

IRRADIATION PERFORMANCE OF WAR FISSILE FUELS 19

THERMODYNAMIC ANALYSIS 41

DISCUSSION AND SUMMARY 45

ACKNOWLEDGMENTS 47

REFERENCES 47

DEVELOPMENT OF A FISSILE PARTICLE FOR HTGR FUEL RECYCLE

F. J. Homan, E. L. Long, Jr., T. B. Lindemer,*
R. L. Beatty, and T. N. Tiegs

ABSTRACT

Recycle fissile fuel particles for high-temperature gas-cooled reactors (HTGRs) have been under development since the mid-1960s. Irradiation performance on early UO_2 and $Th_{0.8}U_{0.2}O_2$ kernels is described in this report, and the performance limitations associated with the dense oxide kernels are presented. The development of the new reference fuel kernel, the weak-acid-resin-derived (WAR) UO_2-UC_2, is discussed in detail, including an extensive section on the irradiation performance of this fuel in HFIR removable beryllium capsules HRB-7 through -10.

The conclusion is reached that the irradiation performance of the WAR fissile fuel kernel is better than that of any coated particle fuel yet tested. Further, the present fissile kernel is adequate for steam cycle HTGRs as well as for many advanced applications such as gas turbine and process heat HTGRs. It is emphasized that throughout this report "fuel" is used in the narrow sense to mean coated particles only, not fuel rods and fuel elements. Further, this report concentrates on kernel development and does not discuss the development associated with the various coating layers on the recycle fissile fuel particle.

INTRODUCTION

Irradiation testing of coated particle fuels has been in progress at ORNL since the mid-1960s.[1] Early work on recycle fuel development was concentrated on oxide systems, because the more difficult fabrication processes associated with the carbide systems are not easily adapted to the remote operation required for fabrication of recycle fuels.

The first candidate recycle fuel for the high-temperature gas-cooled reactor (HTGR) was UO_2. Early irradiation testing of UO_2 identified a severe problem with thermal migration of the UO_2 kernel up the temperature gradient (amoeba), and through the coating layers. The candidate fertile fuel for recycle application has always been ThO_2. The acceptable performance of ThO_2 relative to UO_2 suggested

*Chemical Technology Division.

dilution of the fissile particle with fertile material. Thus, $Th_{0.8}U_{0.2}O_2$ became the reference recycle fuel and was extensively tested. The irradiation tests showed that the thermal stability of $Th_{0.8}U_{0.2}O_2$ was marginal. Higher Th/U ratios were briefly considered for the recycle fissile particle, including Th/U = 8, the maximum dilution possible as it is the overall Th/U ratio in the recycle element. These fuels did not show any decrease in thermal migration rate over the reference $Th_{0.8}U_{0.2}O_2$ fuel.

While the $Th_{0.8}U_{0.2}O_2$ kernels were being irradiation tested under the Thorium Utilization Program, an effort to develop alternate fissile fuels was in progress at ORNL under the HTGR Base Program. One fuel that appeared to have promise was an undiluted fissile fuel derived by loading weak-acid ion exchange resins with uranium from a solution. This weak-acid resin (WAR) fuel had been tested in several irradiation capsules and had performed well. Besides the superior irradiation performance relative to the $Th_{0.8}U_{0.2}O_2$ fuel, there appeared to be some cost advantages to an undiluted fissile fuel; consequently the WAR particle became the reference fissile recycle particle. Additional irradiation testing has confirmed its superiority and has suggested that the WAR fissile fuel may be adequate for use in advanced HTGR applications such as the gas turbine and process heat applications.

The potential cost advantages mentioned above are mainly due to the reduced amount of heavy metal that must be processed in the remotely operated equipment of the refabrication facility. Refabrication of mixed-oxide fuel with Th/U = 4 would require five times as much heavy metal to be processed in the heavily shielded refabrication facility as would be required by an undiluted fissile particle (like the WAR fuel). The use of an undiluted fissile particle permits the fertile fuel to be processed in a contact facility with the coated fertile particles added to the refabrication stream at the blending step. Thus, the expensive remote kernel preparation and coating steps are required only for the fissile material. With the WAR fuel, many of the size and shape separation operations can be done with the unloaded resin in contact equipment with further cost savings. However, it should be emphasized that the WAR fuel was selected as the recycle reference fissile fuel on the basis of superior irradiation performance. The cost advantages are speculative, and require further evaluation.

EARLY WORK WITH OXIDE SYSTEMS AND PERFORMANCE LIMITATIONS OF OXIDE FUELS

The first candidate recycle fuel for the HTGR was UO_2. Early irradiation testing of UO_2 showed a severe problem with thermal migration of the UO_2 kernel up the temperature gradient (also called the amoeba effect), and through the coating layers (Fig. 1). The temperature and temperature gradient[1,2] to which these particles were exposed were nearly equivalent to those in the large high-temperature gas-cooled reactor core design (Fig. 2 and Table 1).

Y-120910

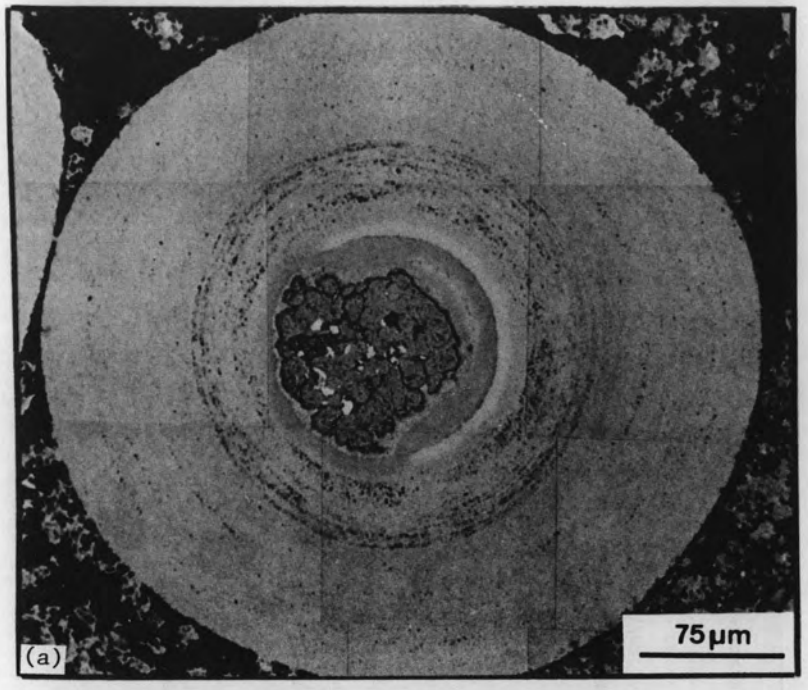

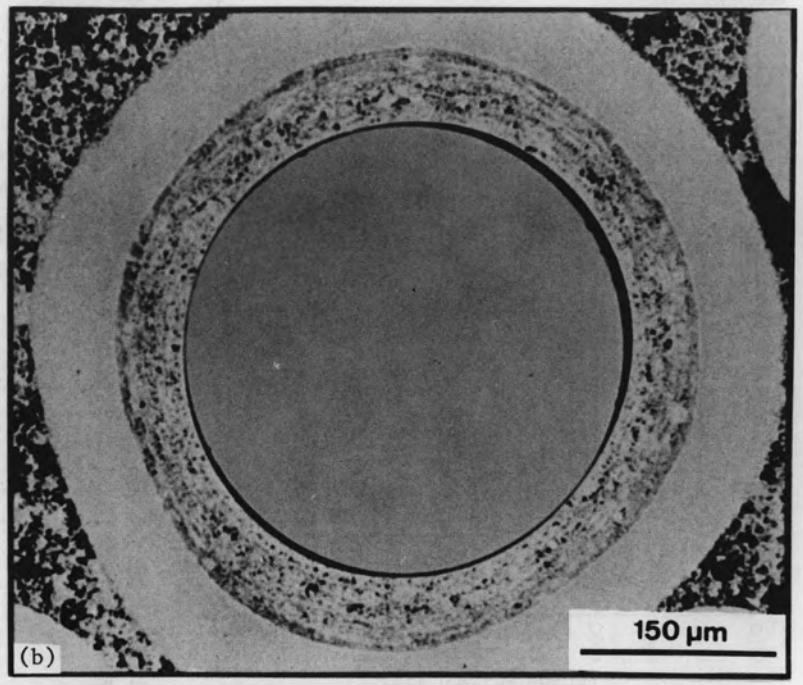

Fig. 1. Relative Thermal Stability of Fissile and Fertile Kernels from Irradiation Test H-1-2. Temperature, 950°C; thermal gradient, 1000°C/cm; fast fluence, 5×10^{21} n/cm^2; time at power, 97 days. (a) UO_2 (33% FIMA). (b) ThO_2 (0.2% FIMA).

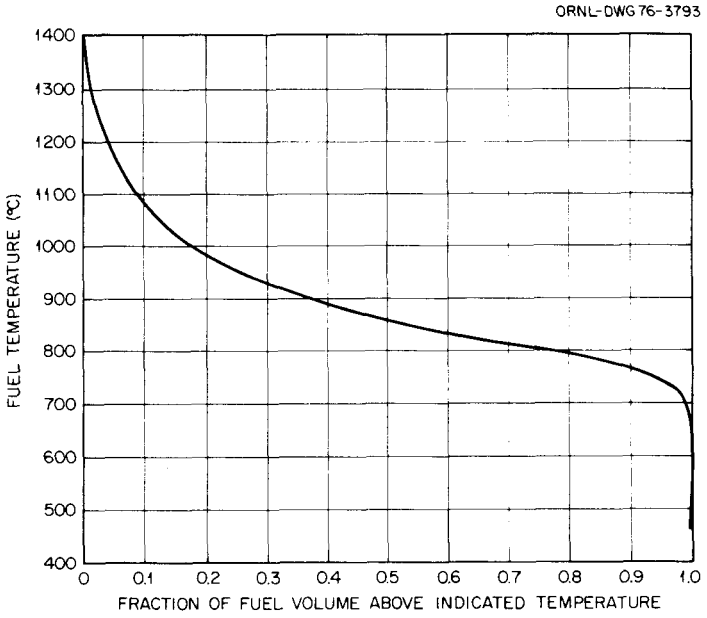

Fig. 2. Fraction of Fuel Operating Above a Given Temperature Under Normal Large HTGR Conditions.

Table 1. Comparison of Temperature and Heat Production Parameters

Parameter	Reactor		
	Fort St. Vrain	Summit Station	Fulton Station
Thermal power, MW	842	2000	3000
Power density, kW/liter	6.3	8.1	8.4
Fuel rod heat rate, kW/m (kW/ft)			
Average	3.9 (1.2)	7.5 (2.3)	7.9 (2.4)
Maximum	12.4 (3.8)	22.3 (6.8)	22.9 (7.0)
Heat flux at coolant holes, W/cm^2			
Average	14.2	20.5	20.5
Maximum	44.2	57.4	58.4
Fuel temperatures, °C			
Volume average	816	857	890
Maximum (short term)	1260	1420	1410
Hot channel		1585	1571
Graphite temperatures, °C			
Average	743	777	739
Maximum	1038	1121	1142
Temperature gradients, °C/cm[a]			
Average		240	250
Maximum		670	700

[a]Based on fuel rod thermal conductivity of 7 $W\ m^{-1}\ K^{-1}$.

The relative thermal stability of UO_2 and ThO_2 may be compared (Fig. 1). The subject of thermal migration has been extensively studied and documented in the technical literature[3,4] and will not be discussed in depth in this report. Only comparisons of the performance of candidate fissile particles for recycle application will be given. Figure 3 compares the average thermal stability of several kernels, among them UO_2 and ThO_2; the upper and lower 90% confidence limits for the data generally lie half an order of magnitude above and below the average. The crosshatched region and above represents unacceptable performance. This region was determined by calculating the kernel migration coefficients that would lead to migration of the kernel through the buffer layer during normal large HTGR operation. In Fig. 3 the UO_2 curve intersects the crosshatched region in the temperature range of primary interest for the large HTGR; whereas the ThO_2 curve is well below the crosshatched area for all temperatures of interest. The UO_2 kernel was therefore rejected.

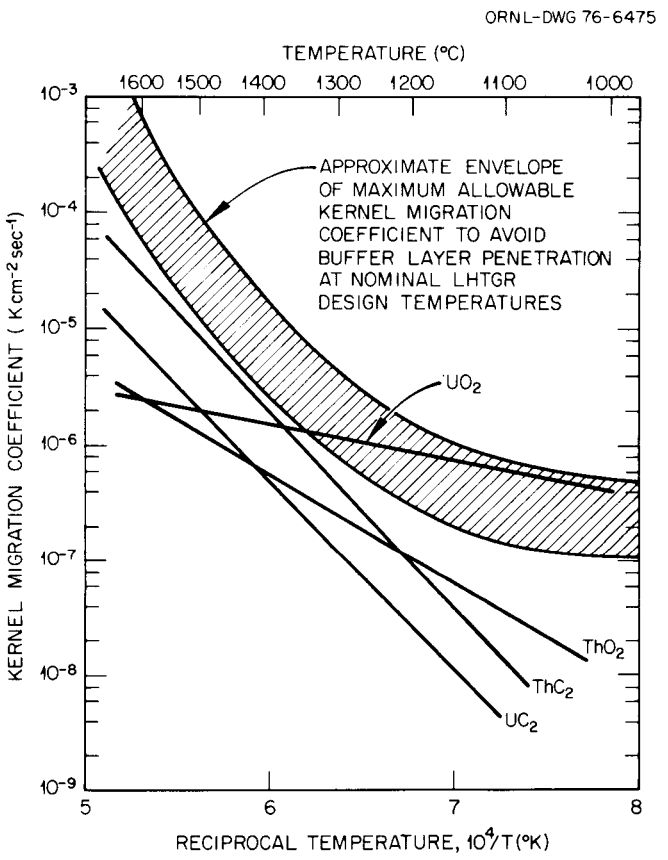

Fig. 3. Average Fuel Kernel Migration Coefficients vs Inverse Temperature Determined from In- and Out-of-Reactor Experiments on Fully Dense Kernels. Source: D. P. Harmon and C. B. Scott, *Development and Irradiation Performance of LHTGR Fuel*, GA-A13173 (October 1975), p. 103.

The favorable performance of ThO_2 relative to UO_2 suggested dilution of UO_2 with enough ThO_2 to stabilize it. Since the overall Th/U ratio in a recycle fuel element is about 8, there seemed to be considerable latitude. Mixed thorium-uranium oxide in the ratio of about 4 was simple to prepare, and the process was thought to be readily adaptable to the remote operation required in HTGR fuel refabrication. The $Th_{0.8}U_{0.2}O_2$ kernel was selected as the reference recycle fissile fuel[5] to replace UO_2, and an irradiation program tested the new reference fuel (Table 2).

Compositions from Th/U = 1 to Th/U = 8 were tested. Initial impressions at modest irradiation temperatures were encouraging (Fig. 4).[6] Very little migration of the $(Th,U)O_2$ occurred and, as before, the ThO_2 was stable. Unfortunately, at higher operating temperatures the $(Th,U)O_2$ was unstable; with the kernel frequently migrating through the coatings (Fig. 5).[7] A significant amount of irradiation data on dense mixed-oxide kernels has been accumulated (Table 2). These data were treated in similar fashion to the UO_2 and ThO_2 data (Fig. 3). The results are given in Fig. 6. The average curve for $Th_{0.8}U_{0.2}O_2$ falls just at the bottom of the crosshatched critical region, in the range 1100–1400°C. However, when the 90% confidence intervals for the thermal migration data are plotted, the upper confidence interval curve extends well into the crosshatched region. This analysis led to the conclusion that this fuel had only marginal thermal stability, so an alternate reference fissile fuel was sought. Additional irradiation testing of other compositions showed little improvement over the reference (Th/U = 4) system (Fig. 7).[8] The thermal stability of the $Th_{0.89}U_{0.11}O_2$ fuel is about the same as that of the $Th_{0.8}U_{0.2}O_2$ fuel.[3]

The fissile particle selected to replace the dense mixed oxide was an undiluted fissile kernel derived from loading uranium into ion-exchange resins from an acid-deficient solution. This weak-acid-resin-derived (WAR) fuel will be discussed in detail in the following sections.

PROCESSING CONSIDERATIONS

The weak-acid-resin-derived (WAR) fissile kernel was selected to replace the $Th_{0.8}U_{0.2}O_2$ kernel as the reference recycle fuel in early 1974. A great deal of optimism existed at that time about the potential for this fuel and the flexibility associated with kernel processing. It was thought that kernel densities ranging from about 2.8 to 5.0 g/cm^3 would be possible, with compositions ranging from UO_2 to UC_2. The expected lower cost has already been discussed. Particle design advantages were also expected. The porosity of the kernel was thought to be sufficient to accommodate fuel swelling, thus reducing or eliminating the need for a buffer layer.

Table 2. Summary of ORNL Experimental Data on Mixed (Th,U) Oxide Recycle Fuel

Part 1. Real-Time Testing Under HTGR Conditions in Peach Bottom Reactor

Irradiation[1,2] experiment No.	Batch No. and fuel type	Th/U ratio	Fast fluence E > 0.18 MeV (n/cm^2)	Average burnup (% FIMA)	Maximum fuel temperature (°C)	Design[a] (μm)	Density[a] (g/cm^3)	Remarks
RTE-1 (FTE-11)								
Body 1	PR-56 PR-66	4:1 2:1	3.3×10^{21}	9.0 14.7	c	350/75/130 350/90/130	10.1/1.1/1.9 10/1.17/1.86	Slug-injected; carbonized in covered graphite tray; to be examined.
Body 2	PR-56 PR-66	4:1 2:1		9.0 14.7		350/75/130 350/90/130	10.1/1.1.1.9 10/1.17/1.86	
Body 3	PR-56 PR-67	4:1 2:1		9.0 14.7		350/75/130 350/90/140	10.1/1.1/1.9 10/1.17/1.85	
Body 4	PR-56 PR-67	4:1 2:1		9.0 14.7		350/75/130 350/90/140	10.1/1.1/1.9 10/1.17/1.85	
Body 5	PR-66	2:1		14.7		350/90/130	10/1.17/1.86	
Body 6	PR-66	2:1		14.7		350/90/130	10/1.17/1.86	
RTE-2								
Body 2	PR-66	2:1	3.6×10^{21}	13.3	1190[d]	350/90/130	10/1.17/1.86	Slug-injected; carbonized in covered graphite tray. Fuel examined from highest temperature region and is considered representative; no amoeba; no indication of failure.
Body 5	PR-55	4:1	3.6×10^{21}	8.2	1300[d]	350/70/80	10.1/1.1/1.9	Loose bed of particles; fuel examined from highest temperature region and is considered representative; no amoeba; no indication of failure.
RTE-4								
Body 3	PR-54	4:1	2.0×10^{21}	5.0	1260[d]	350/70/70	10.1/1.1/1.94	Loose bed of particles; fuel examined from highest temperature region and is considered representative; no amoeba; no indications of failure.
Body 5	PR-61	2:1	2.0×10^{21}	8.5	1230[d]	350/75/120	10.2/1.16/1.91	Slug-injected; carbonized in covered graphite tray; fuel examined from highest temperature region and is considered representative; no amoeba; no indication of failure.
RTE-5								
Body 1	PR-57-1 PR-61	4:1 2:1	4.6×10^{21}	11.9 18.4	c	350/75/135 350/75/120	10.1/1.1/1.9 10.2/1.16/1.9	Slug-injected; carbonized in covered graphite tray; to be examined.
Body 2	PR-57-1 PR-61	4:1 2:1		11.9 18.4		350/75/135 350/75/120	10.1/1.1/1.9 10.2/1.16/1.9	
Body 3	PR-57-1 PR-61	4:1 2:1		11.9 18.4		350/75/135 350/75/120	10.1/1.1/1.9 10.2/1.16/1.9	
Body 4	PR-57-1 PR-61	4:1 2:1		11.9 18.4		350/75/135 350/75/120	10.1/1.1/1.9 10.2/1.16/1.9	
Body 5	PR-60	2:1		18.4		350/75/120	10.2/1.16/1.9	
Body 6	PR-60	2:1		18.4		350/75/120	10.2/1.16/1.9	
RTE-6								
Body 3	PR-60	2:1	4.6×10^{21}	18.2	c	350/75/120	10.2/1.16/1.9	Slug-injected;carbonized in covered graphite tray; fuel examined from highest temperature region and is considered representative; no amoeba; no indication of failure.
RTE-8								
Body 4	PR-60	2:1	4.6×10^{21}	18.1	c	350/75/120	10.2/1.16/1.9	Slug-injected; carbonized in covered graphite tray.
RTE-7								
Body 1	PR-60	2:1	1.3×10^{21}	5.5	880[d]	350/75/120	10.2/1.16/1.9	Slug-injected; carbonized in covered graphite tray; fuel examined from highest temperature region and is considered representative; no amoeba; no indications of failure.
Body 2	PR-60	2:1		5.5	1130[d]	350/75/120	10.2/1.16/1.9	
Body 3	PR-60	2:1		5.5	1230[d]	350/75/120	10.2/1.16/1.9	
Body 4	PR-60	2:1		5.5	1230[d]	350/75/120	10.2/1.16/1.9	
Body 5	PR-57-1 PR-57-6 PR-61	4:1 4:1 2:1		3.2 3.2 5.5	1150[d] 1150[d] 1150[d]	350/75/135 350/75/135 350/75/120	10.1/1.1/1.9 10.1/1.1/1.9 10.2/1.16/1.9	
Body 6	PR-57-1 PR-61	4:1 2:1		3.2 5.5	1050[d] 1050[d]	350/75/135 350/75/120	10.1/1.1/1.9 10.2/1.16/1.9	

Table 2 — Part 2. Accelerated Testing in Research Reactors

Fissile particle batch No.	Sample identification	Fast fluence E > 0.18 MeV (n/cm²)	Burnup (% FIMA)	Th/U Ratio	Design A/B/C/D/E (μm)	Density A/B/C/D/E (μm)	Maximum fuel temperature (°C)
				H-1[3]			
PR-57	H-1-4	6.3×10^{21}	8.2	4:1	355/80/135	10.1/1.1/1.92	1420[e]
	H-1-10	5.4	8.6	4:1	355/80/135	10.1/1.1/1.92	2150[e]
	H-1-6	8.6	8.6	4:1	355/80/135	10.1/1.1/1.92	1670[e]
PR-67	H-1-3	5.8×10^{21}	12.0	2:1	350/80/140	10/1.1/1.85	1370[e]
	H-1-11	4.5	12.0	2:1	350/80/140	10/1.1/1.85	2390[e]
				H-2[7]			
PR-57	H-2-4	7.5×10^{21}	7.5	4:1	355/80/135	10.1/1.1/1.92	1430[e]
	H-2-10	8.3	8.3	4:1	355/80/135	10.1/1.1/1.92	1800[e]
	H-2-6	8.2	8.2	4:1	355/80/135	10.1/1.1/1.92	1690[e]
PR-67	H-2-3	5.2×10^{21}	11.0	2:1	350/80/140	10/1.1/1.85	1350[e]
	H-2-11	4.1	12.0	2:1	350/80/140	10/1.1/1.85	1910[e]
				HRB-1[4]			
YZ-233	1A	2.9×10^{21}	9.8	4:1	195/37/20/33/53	3.4/?/?/3.11/1.8	
	1B	2.9	9.8		195/37/20/33/53		
	1C	2.9	9.8		195/37/20/33/53		770[f]
	2A	3.4	10.2		195/37/20/33/53		
	3A	4.8	12.7		195/37/20/33/53		
	3B	4.8	12.7		195/37/20/33/53		1150[f]
	4A	5.3	13.8		195/37/20/33/53		1400[f]
	5A	5.8	14.9		195/37/20/33/53		1130[f]
	5B	5.8	14.9		195/37/20/33/53		
	6A	5.4	14.0		195/37/20/33/53		
	6B	5.4	14.0		195/37/20/33/53		1140[f]
				HRB-6[5]			
OR-1910	1A	5.8×10^{21}	23.8	4:1	350/100/30/25/40	10/1.15/1.95/3.2/1.95	
OR-1909	1B	6.8	25.8		350/100/30/25/40	10/1.15/1.95/3.2/1.95	1190[g]
PU-291	3A	7.2	26.7		350/100/80	10/1.15/1.95	1220[g]
OR-1909	3B	6.7	26.0		350/100/90	10/1.15/1.95	1200[g]
Pu-291	3C	6.1	25.0		350/100/80	10/1.15/1.95	1300[g]
OR-1909	3D	5.4	23.6		350/100/90	10/1.15/1.95	1250[g]
				HRB-7[6,7]			
J-263	2	4.07×10^{21}	20.8	4:1	350/100/100	10/1.3/2.0	1500[h]
OR-2094H	8	6.04	32.8	2:1	300/85/85	10/1.2/1.95	
OR-2116H	9	6.14	22.5	4:1	350/100/30/30/40	10/1.2/1.95/3.18/1.95	
GGA-6155-01-020	10	6.14	16.4	8:1	500/100/30/30/40	10/1.2/1.95/3.18/1.8	
OR-2111H	11	6.14	21.7	4:1	350/90/100	10/1.2/2.00	
OR-2090H	12	6.04	43.9	1:1	250/85/85	10/1.2/1.95	
J-263	19	3.62	18.9	4:1	350/100/100	10/1.3/2.0	
				HRB-8[6,7]			
J-263	2	5.35×10^{21}	21.4	4:1	350/100/100	10/1.3/2.0	1250[h]
OR-2094-H	8	7.95	34.0	2:1	350/85/85	10/1.2/1.95	
OR-2116-H	9	8.09	25.3	4:1	350/100/30/30/40	10/1.2/1.95/3.18/1.95	
GGA-6155-01-0RO	10	8.09	19.4	8:1	500/100/30/30/40	10/1.2/1.95/3.18/1.8	
OR-2111-H	11	8.09	24.6	4:1	350/90/100	10/1.2/2.00	
OR-2090-H	12	7.95	45.7	1:1	250/85/85	10/1.2/1.95	
J-263	19	4.78	18.8	4:1	350/100/100	10/1.3/2.0	
				HRB-9[6]			
OR-2116H	2	5.25×10^{21}	21.2	4:1	350/100/30/30/40	10/1.2/1.95/3.18/1.95	1250[h]
OR-2116H	7	7.57	24.4	4:1	350/100/30/30/40	10/1.2/1.95/3.18/1.95	1250[h]
				HRB-10[6]			
OR-2116H	2	3.3×10^{21}	18.4	4:1	350/100/30/30/40	10/1.2/1.95/3.18/1.95	1500[h]
OR-2116H	7	4.8	20.5	4:1	350/100/30/30/40	10/1.2/1.95/3.18/1.95	1500[h]
				OF-1[7]			
J-263	Rod 1-1	10.8×10^{21}	19.0	4.2:1	350/100/100	10/1.1/2.0	1200[h]
	1-2	9.58	18.1				
	1-3	8.00	16.9				
	1-4	5.72	15.9				
J-263	2-1	9.85	18.3				
	2-2	8.61	17.5				
	2-3	6.99	16.4				
	2-4	4.88	15.5				
OR-1977	3-1	9.85	16.9				
OR-1977	3-2	8.61	16.1				
J-263	3-3	7.40	16.7				
J-263	3-4	5.92	16.0				
J-263	3-5	4.37	15.3				
J-263	4-1	10.8	19.0				
	4-2	9.58	18.1				
	4-3	8.00	16.9				
	4-4	5.72	15.9				
Pu 291[a]	5-1	10.4	20.2[a]				
OR 1977	5-2	9.18	16.4				1350[h]
Pu 291[a]	5-3	7.48	18.1[a]				1350[h]
OR 1977	5-4	5.25	14.4				1350[h]

Table 2 — Part 2a.

Fissile particle batch No.	Sample identification	Remarks
		H-1
PR-57	H-1-4	Only failures noted in single plane of polish viewed were due to fabrication defects.
	H-1-10	Very high temperatures during fourth cycle; extensive damage at center of rod.
	H-1-6	Loose particles. Amoeba related failures.
PR-67	H-1-3	Only slight evidence of amoeba; no failed coatings.
	H-1-11	Rod debonded into large fragments; damaged particles on surface of rod.
		H-2
PR-57	H-2-4	Not examined; sent to Chemical Technology Division for reprocessing studies.
	H-2-10	Center badly damaged due to very high temperature during last cycle.
	H-2-6	Loose particles. Not examined.
PR-67	H-2-3	Fuel rod debonded; no failed particles observed during visual examination.
	H-2-11	Outer surfaces of particles near the surface of rod chemically attacked; amoeba apparent; kernel migrated through buffer and into LTI.
		HRB-1
YZ-233	1A	Slug-injected rods; thin two-component sacrificial layer on outer surface of particles caused debonding of rods with low-density matrix (1A, 1B, 1C, 2A, 4A, 4B). Metallography showed no failed particles or amoeba.
YZ-233	1B	
YZ-233	1C	
YZ-233	2A	
YZ-233	3A	
YZ-233	3B	
YZ-233	4A	
YZ-233	5A	
YZ-233	5B	
YZ-233	6A	
YZ-233	6B	
		HRB-6
OR-1910	1A	Extruded rod; no failures; no amoeba; intermittent plastic flow through recoil zone.
OR-1909	1B	Extruded rod; no failures; slight amoeba (2—3 μm); intermittent plastic flow through recoil zone.
Pu-291*	3A	Slug-injected; carbonized in packed Al_2O_3; > 50% failed; amoeba (20 μm); failures attributed to defective coatings.
OR-1909	3B	Slug-injected; carbonized in packed Al_2O_3; no failures; amoeba (20 μm).
Pu-291*	3C	Slug-injected; carbonized in packed Al_2O_3; visual examination only; no broken particles.
OR-1909	3D	Slug-injected; carbonized in packed Al_2O_3; visual examination only; no broken particles.
		HRB-7
J-263	2	Slug-injected; carbonized in packed Al_2O_3; no failures; amoeba ($\leq$ 40 μm).
OR-2094H	8	Slug-injected; carbonized in packed Al_2O_3; no failures; amoeba ($\leq$ 80 μm).
OR-2116H	9	Slug-injected; carbonized in packed Al_2O_3; no failures; amoeba ($\leq$ 25 μm).
GGA-6155-01-020	10	Slug-injected; carbonized in packed Al_2O_3; 12% failed; amoeba ($\leq$ 25 μm).
OR-2111H	11	Slug-injected; carbonized in packed Al_2O_3; no failures; ampeba ($\leq$ 75 μm).
OR-2090H	12	Slug-injected; carbonized in packed Al_2O_3; no failures; amoeba ($\leq$ 55 μm).
J-263	19	Slug-injected; carbonized in packed Al_2O_3; no failures; amoeba ($\leq$ 30 μm).
		HRB-8
J-263	2	Slug-injected; carbonized in packed Al_2O_3; no failures; amoeba ($\leq$ 13 μm).
OR-2094-H	8	Slug-injected; carbonized in packed Al_2O_3; no failures; amoeba ($\leq$ 20 μm).
OR-2116-H	9	Slug-injected; carbonized in packed Al_2O_3; no failures; amoeba ($\leq$ 25 μm).
GGA-6155-01-020	10	Slug-injected; carbonized in packed Al_2O_3; no failures; amoeba ($\leq$ 85 μm).
OR-2111-H	11	Slug-injected; carbonized in packed Al_2O_3; no failures; amoeba ($\geq$ 20 μm).
OR-2090-H	12	Slug-injected; carbonized in packed Al_2O_3; 13% failed; amoeba ($\leq$ 55 μm).
J-263	19	Slug-injected; carbonized in packed Al_2O_3; no failures; amoeba ($\leq$ 20 μm).

Table 2 — Part 2a. (Continued)

Fissile particle batch No.	Sample identification	Remarks
		HRB-9
OR-2116H	2	Slug-injected; carbonized in packed Al_2O_3; visual examination only; no broken particles.
OR-2116H	7	Slug-injected; carbonized in packed Al_2O_3; visual examination only; no broken particles.
		HRB-10
OR-2116H	2	Slug-injected; carbonized in packed Al_2O_3; visual examination only; no broken particles.
OR-2116H	7	Slug-injected; carbonized in packed Al_2O_3; no failures; amoeba ($\leq$ 35 μm).
		OF-1
J-263	1-1	Slug-injected; no failures (Metallography); amoeba ($\leq$ 5 μm); carbonized in packed Al_2O_3.
	1-2	Slug-injected; stereo-examination only; no broken particles; carbonized in packed Al_2O_3.
	1-3	Slug-injected; stereo-examination only; no broken particles; carbonized in packed Al_2O_3.
	1-4	Slug-injected; stereo-examination only; no broken particles; carbonized in packed Al_2O_3.
J-263	2-1	Slug-injected; stereo-examination only; no broken particles; carbonized in graphite block.
	2-2	Slug-injected; no failures (Metallography); amoeba ($\leq$ 5 μm); carbonized in graphite block.
	2-3	Slug-injected; stereo-examination only; no broken particles; carbonized in graphite block.
	2-4	Slug-injected; stereo-examination only; no broken particles; carbonized in graphite block.
OR-1977	3-1	Slug-injected; stereo-examination only; no broken particles; carbonized in packed Al_2O_3.
OR-1977	3-2	Slug-injected; no failures (Metallography); amoeba ($\leq$ 20 μm); carbonized in packed Al_2O_3.
J-263	3-3	Slug-injected; stereo-examination only; no broken particles; carbonized in packed Al_2O_3.
J-263	3-4	Slug-injected; no failures (Metallography); no amoeba; carbonized in packed Al_2O_3.
J-263	3-5	Slug-injected; stereo-examination only; no broken particles; carbonized in packed Al_2O_3.
J-263	4-1	Slug-injected; no failures (Metallography); amoeba ($\leq$ 20 μm); carbonized in graphite block.
J-263	4-2	Slug-injected: stereo-examination only; 3 broken particles on surface (identity unknown); carbonized in graphite block.
J-263	4-3	Slug-injected; stereo-examination only; no broken particles; carbonized in graphite block.
J-263	4-4	Slug-injected; stereo-examination only; no broken particles; carbonized in graphite block.
Pu-291[i]	5-1	Slug-injected; ~ 80% failed (Metallography); carbonized in packed Al_2O_3; ($\leq$ 15 μm); failures attributed to defective coatings.
OR-1977	5-2	Slug-injected; no failures (Metallography) carbonized in packed Al_2O_3; no amoeba.
Pu-291[i]	5-3	Slug-injected; ~ 15% failed (Metallography); carbonized in packed Al_2O_3; amoeba (< 10 μm); failures attributed to defective coatings.
OR-1977	5-4	Slug-injected; stereo-examination only; carbonized in packed Al_2O_3; no broken particles.

[a]A = kernel; B = buffer; C = IPyC; D = SiC; E = OPyC.

[b]Approximately 11,000 to 18,000 fissile particles per rod in RTE fuel rods, depending on particle diameter and density. Forty-eight fuel rods per body.

[c]Thermal analysis to be completed by July 1976.

[d]Maximum fuel temperature in fuel body. These are estimated temperatures based on as-fabricated dimensions. Detailed analyses incorporating irradiation-induced dimensional changes are being performed.

[e]These temperatures represent the maximum calculated for the fuel rod centerline during the irradiation. This experiment was complicated by a nonintentional inversion of the capsule during the last of four irradiation cycles. (See ref. 4 for additional details on fuel operating temperatures.)

[f]Temperatures for HRB-1 were calculated from readings from thermocouples adjacent to fuel rods. Centerline temperatures were calculated by assuming a fuel rod conductivity of 3.0 Btu/hr-ft-°F and a radial gap of 0.004 in. Fuel rod 4B was composed of a resin binder, and the matrix debonded rather badly during irradiation. Therefore, the thermal conductivity of the fuel rod may have been as low as 1.5 Btu/hr-ft-°F (a value associated with loose beds of particle). This change in the bed conductivity increases the calculated fuel centerline temperature from 1230 to 1430°C.

[g]From detailed thermal analysis (ref. 5).

[h]Maximum design fuel temperatures.

[i]Fueled with ^{233}U.

References

[1]E. L. Long, Jr. et al., *Fabrication of ORNL Fuel Irradiated in the Peach Bottom Reactor and Postirradiation Examination of Recycle Test Elements 7 and 4*, ORNL-TM-4477 (September 1974).

[2]R. P. Morissette and K. P. Steward, *Recycle Test Element Program Design, Fabrication, and Assembly*, GA-10109 (September 1971).

[3]R. A. Olstad et al., *An Irradiation Test of Candidate HTGR Recycle Fuels in the H-1 and H-2 Capsules*, ORNL-TM-4397 (July 1974).

[4]J. L. Scott et al., *An Irradiation Test of Bonded HTGR Coated Particle Fuels in an Instrumented Capsule in HFIR*, ORNL-TM-3640 (March 1972).

[5]F. J. Homan et al., *Irradiation Performance of HTGR Fuel Rods in HFIR Experiment HRB-6*, ORNL-TM-5011 (December 1975).

[6]K. H. Valentine et al., *Irradiation Performance of HTGR Fuel Rods in HFIR Experiments in HRB-7 and -8*, in preparation.

[7]*HTGR Base Program Progr. Rep. Jan. 1, 1974 to June 30, 1975*, ORNL-5108, in preparation.

Y-120917

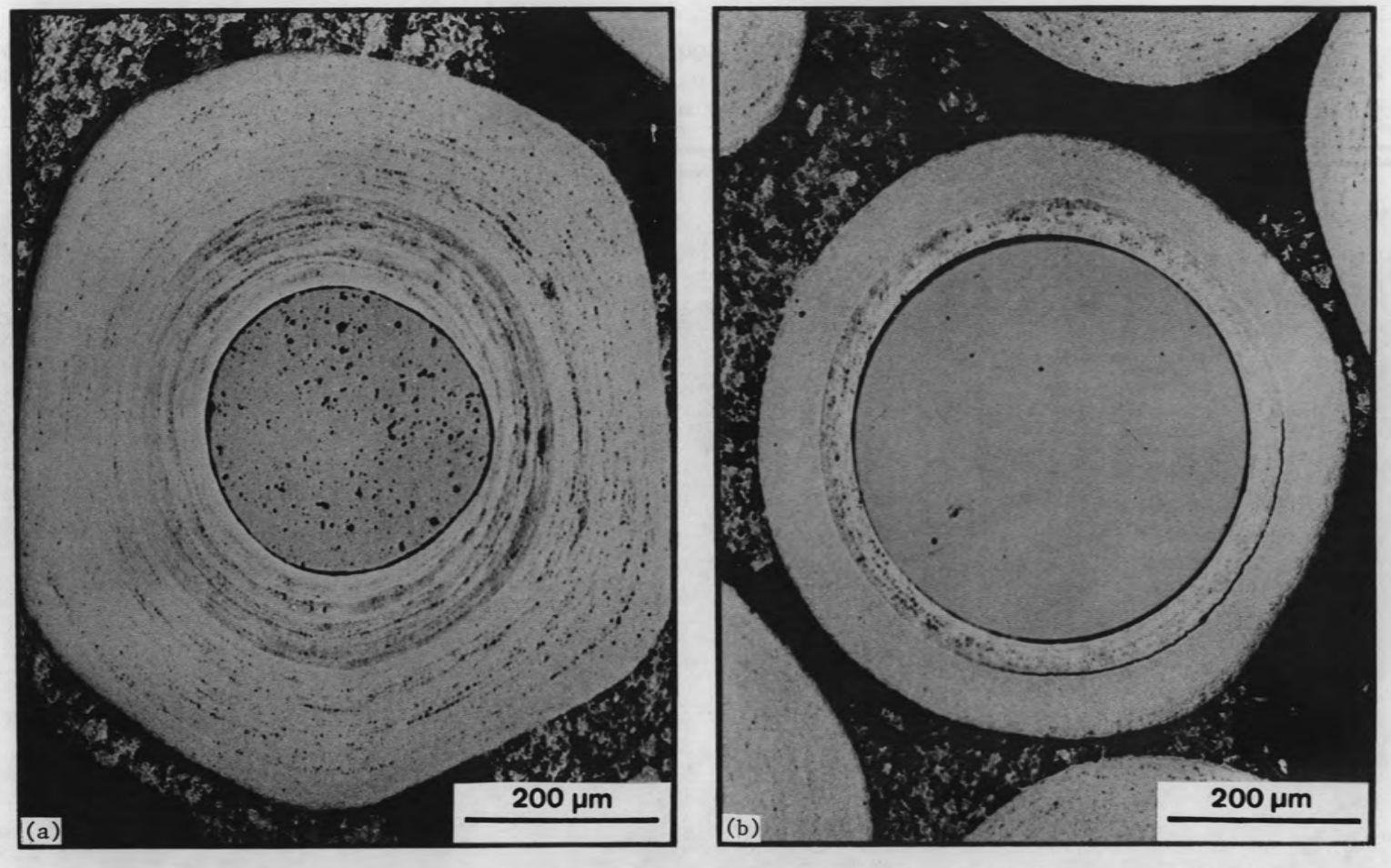

Fig. 4. Relative Thermal Stability of Fissile and Fertile Particles in Irradiation Test H-1-4. Temperature, 1050°C; thermal gradient, 1200°C/cm; fast fluence, 6.3×10^{21} n/cm^2; time at power, 134 days. (a) $(4.1Th,U)O_2$ (8.2% FIMA). (b) ThO_2 (0.4% FIMA).

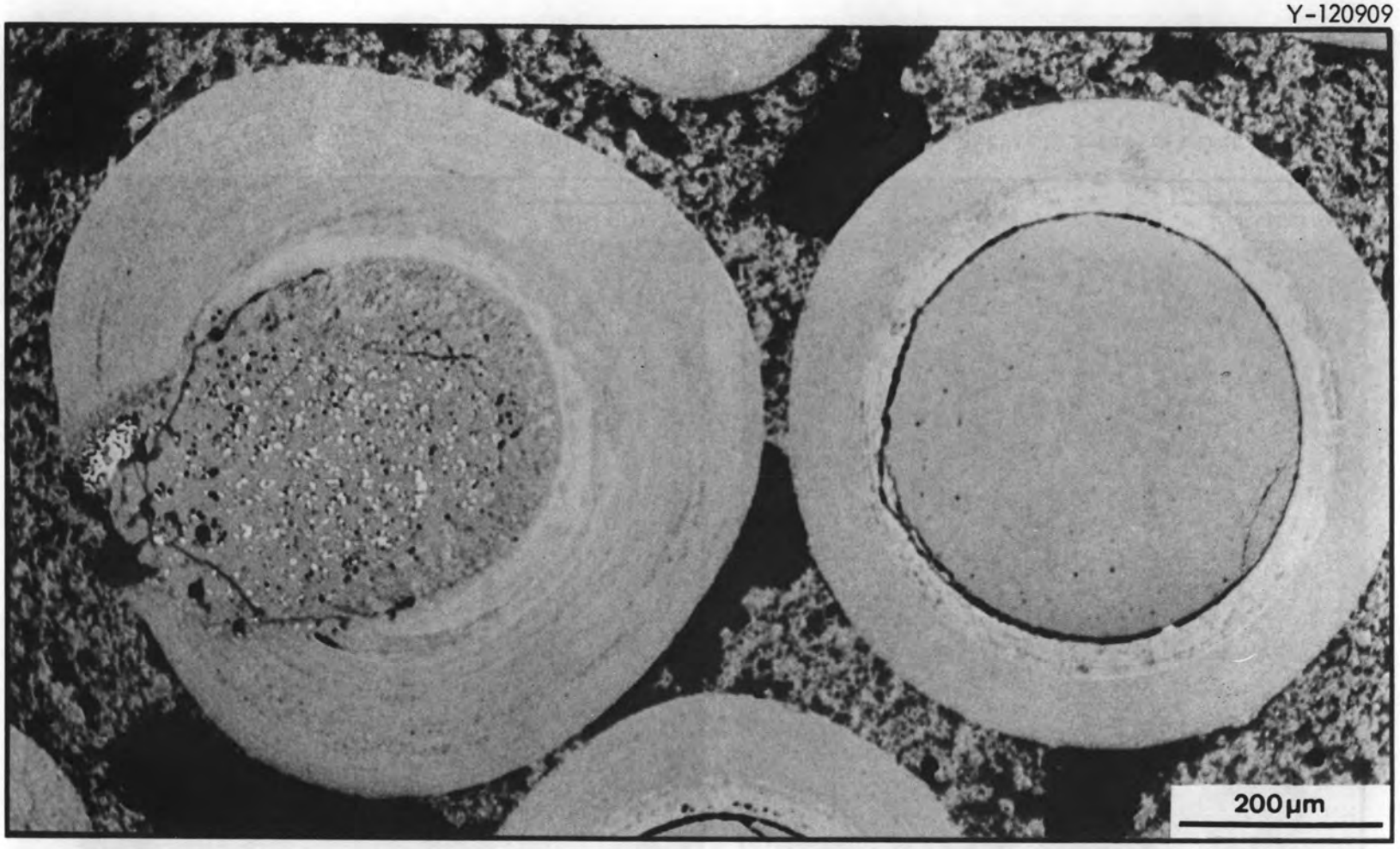

Fig. 5. Relative Thermal Stability of Fissile and Fertile Kernels in Irradiation Test H-2-10. Temperature, 1350°C; thermal gradient, 1700°C/cm; fast fluence, 5×10^{21} n/cm^2; time at full power, 37 days. Left: $(4Th,U)O_2$ (8.3% FIMA). Right: ThO_2 (0.3% FIMA).

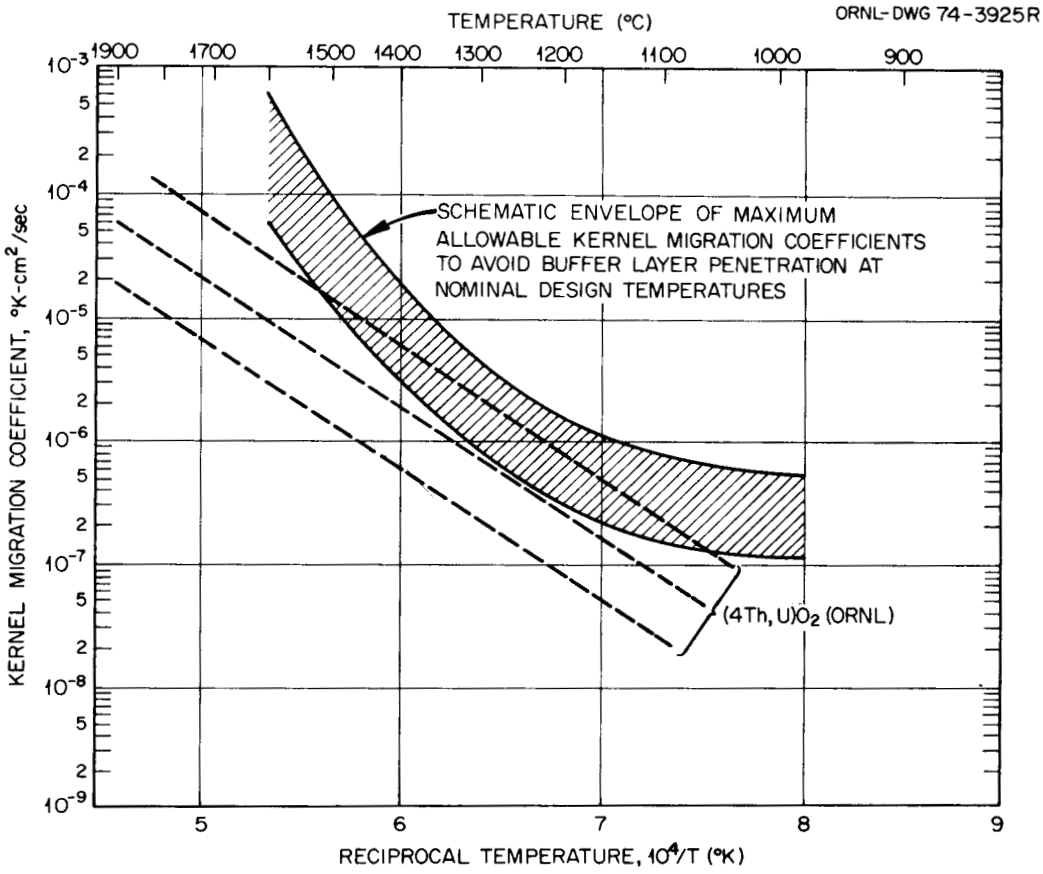

Fig. 6. Average Kernel Migration Coefficients for $(4Th,U)O_2$.

R-65778

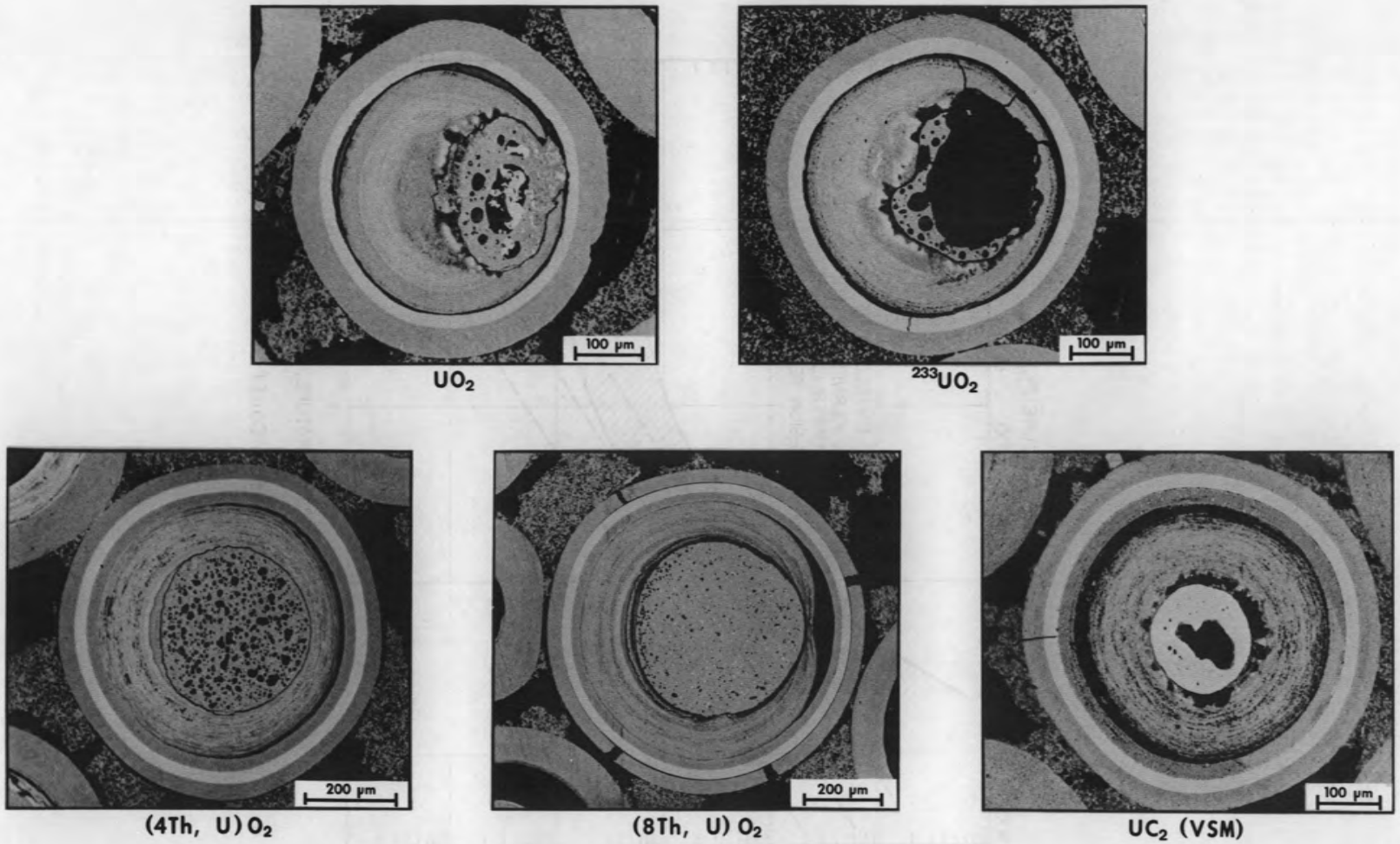

Fig. 7. Relative Thermal Stability of HTGR Candidate Recycle Oxide vs Reference UC_2 Fissile Particles. 4–6 × 10^{21} n/cm^2 (>0.18 MeV); 80% FIMA; 1500°C design centerline temperature.

It should be emphasized that while only limited irradiation data existed on WAR fuel in early 1974 a considerable amount of data existed on resin-based fuel systems. This data included evaluation of several ion-exchange resins; various uranium-loading schemes; effects of varying carbonization cycles; control of conversion or reduction to carbide; and atmospheric requirements for handling, coating, and irradiation testing.[9–14] Recent development effort has been concentrated on WAR fuel employing acrylic acid-divinylbenzene copolymers, Amberlite IRC-72, manufactured by Rohm and Haas, and Duolite C-464, manufactured by Diamond Shamrock. Resin particles in Na^+ form are obtained without upgrading for size or shape. The bulk of the particles are spherical, but are distributed over a broad range of sizes. The material is wet-screened to obtain the size fraction required, about 600 to 800 μm in the wet Na^+ form, dried, and shape separated on vibrating trays to remove the nonspherical fraction. Yield of sized spheres is about 20% of as-received resin. This ability to thoroughly upgrade unfueled particles by a contact process before loading the uranium is a major advantage of the resin process for fuel recycle since all operations involving recycle fuel must be done remotely. The sized microspheres are then remoistened and converted to H^+ form for loading of uranium.

Of the many possible schemes for loading uranium, all studied extensively at ORNL employ H^+ form resin and thus require acid-deficient loading liquors. The currently favored process uses uranyl nitrate with acid deficiency maintained by amine extraction.[3] Reaction equilibrium is maintained to favor the replacement of H^+ pairs by UO_2^{2+} ions to achieve essentially 100% loading of resin capacity. After the resin is fully loaded it is washed and dried at 110°C.

Fabrication of fuel kernels from dried resin involves carbonization of the resin structure followed by conversion or reduction to adjust the oxygen content. Product properties are sensitive to control in both steps. Both carbonization and conversion are carried out in an argon-fluidized bed, which allows the necessary control of temperature, heating rate, and atmosphere. Varying the carbonization cycle, specifically the rate of heating between 350 and 450°C, has a critical effect on density and carbon content of the final product. Critical carbonization reactions of the resin are nearly complete at 450°C, and the residual carbon yield increases strongly with decreasing rate of heating to that point; heating rate above 450°C is relatively unimportant. Weight loss, volume shrinkage, and the carbon-to-uranium ratio (C/U) of the carbonized product vary with heating rate through the critical range between 350 and 450°C for the Amberlite resin (Fig 8). Thus, considerable flexibility is available to tailor properties of the product since uranium-loaded WAR can be heated through the critical range at rates as high as 300°C/min without destroying microsphere integrity. The carbonized material, after heating to 1200°C, can have densities ranging from about 2.8 to 3.8 g/cm^3 and C/U ranging from about 4 to 6, depending on carbonization rate. Slow carbonization results in more porosity as well as more retained carbon to give lower

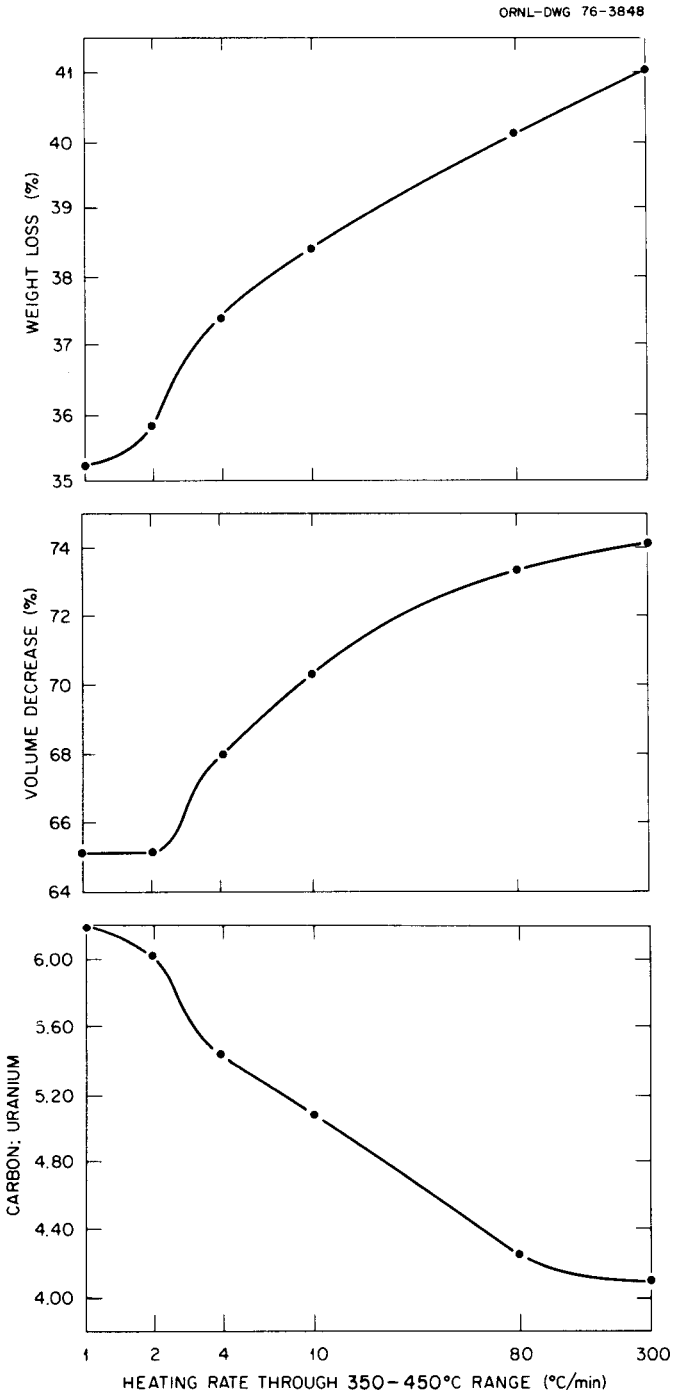

Fig. 8. Effect of Critical Range (350–450°C) Heating Rate on Carbonization of Uranium-Loaded Weak-Acid Resin (Amberlite IRC-72) Carbonized to 1200°C.

density. After carbonization, the material formula may be written as $UO_2 + nC$, where n varies from 4 to 6. The fuel phase is poorly crystalline UO_2 finely dispersed in a porous glassy carbon matrix. The kernels may be coated at this point if oxide fuel is desired.

If carbide or mixed oxide-carbide fuel is desired, conversion is effected by heating in the argon-fluidized bed. Residual carbon from the resin is sufficient for complete carbothermic reduction, and again the process is very flexible in allowing control of product properties. The fluidized bed offers excellent control of reduction rate as long as the microspheres are well fluidized and do not sinter appreciably. Since the carbonized material has an extensive system of interconnected porosity, reduction rate is limited, not by solid-state diffusion, but by rate of carbon monoxide removal. The carbon monoxide partial pressure in the bed is fixed at approximately the equilibrium P_{CO} for the reaction:

$$UO_2 + 4C \rightarrow UC_2 + 2CO \ ,$$

or

$$UO_2 + 3C \rightarrow UC + 2CO \ .$$

The difference in equilibrium P_{CO} for the above reactions is not significant relative to experimental error in temperature control. The reaction rate can be calculated from

$$f_{CO} = P_{CO} f_{Ar} / (P_{total} - P_{CO}) \ ,$$

where

f_{CO} = evolving carbon monoxide flow rate,

f_{Ar} = flow rate of argon,

P_{total} = atmospheric pressure, and

P_{CO} = equilibrium P_{CO} for temperature employed.

For the 1500–1600°C range commonly used, where P_{CO} is less than 4% of atmospheric pressure, the reaction rate can be adequately predicted from

$$f_{CO} = P_{CO} f_{Ar} / P_{total} \ .$$

Thus, reduction rate is predictably controlled by temperature and specific argon flow rate (Fig. 9) as long as interconnected porosity is retained.[15] Whether microspheres densify and lose this porosity depends sensitively on the C/U (i.e., early carbonization rate). If the C/U after carbonization is near 6, the material does not densify on conversion to carbide,

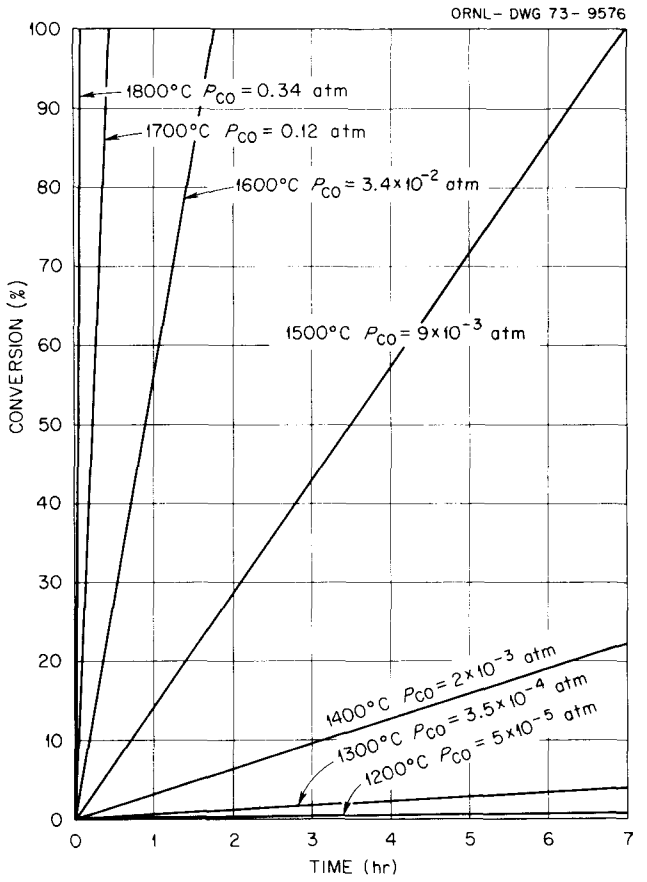

Fig. 9. Fluidized-Bed Conversion of Uranium-Loaded Weak-Acid Resin from Oxide to Carbide. (Assumed equilibrium P_{CO} for reaction $UO_2 + 3C \rightarrow UC + 2CO$. Normalized to 0.05 liter/min of sweep gas per g of U.)

and the reduction rate is essentially linear with time to completion. On the other hand, if C/U after carbonization is less than about 5.6, the microspheres begin to sinter after partial reduction so reduction rate is not readily predictable. Sintering, of course, does not preclude complete reduction, and dicarbide particles of density greater than 6.0 g/cm^3 can be produced this way. However, if a low-density (~3.0 g/cm^3) dicarbide or a controlled oxide-carbide composition is the desired product, the process must be suitably regulated throughout. To avoid particle densification at high temperatures, a heating rate of 2°C/min or slower is necessary through the 350–450°C range. Given this restriction the WAR process is ideally suited to production of any oxide-carbide composition. The significance of this process capability will be discussed later. At this stage the kernel consists of UO_2, UC_2, and free carbon and the material formula may be written as UC_xO_y, where y varies from 0 to 2 and x from about 2.5 to 6. Major fuel phases present in partially converted WAR fuel are UO_2 and UC_2. A nonequilibrium minor phase, UC_xO_{1-x}, may be present in partially converted fuel, depending on the conversion process control exercised, but this phase will decompose to UO_2 and UC_2 in subsequent processing or in the reactor.

IRRADIATION PERFORMANCE OF WAR FISSILE FUELS

The decision to switch from $Th_{0.8}U_{0.2}O_2$ to WAR UC_xO_y as the reference recycle fissile kernel was based on the performance of WAR fuel in the HRB-4 and -5 capsules (Table 3).[16] Typical postirradiation metallography of the WAR fuel irradiated in those capsules is shown in Figs. 10 and 11. Extensive testing of WAR-derived fuels was conducted in HFIR capsules HRB-7 and -8 (ref. 17) and capsules HRB-9 and -10 (ref. 18). In these capsules direct comparisons were made between the performance of WAR fuels of various compositions, and dense mixed-oxide fuels, as well as with the reference HTGR fresh fuel (dense UC_2).

Conclusions about WAR fuel performance from this accelerated testing are summarized:

1. The porous WAR kernels densify considerably under irradiation (Fig. 10). The density of the WAR kernels is typically about 3 g/cm^3 before irradiation, compared with densities greater than 10 g/cm^3 for the dense mixed-oxide kernels described earlier. Frequently the densified WAR kernels remain attached to one side of the coating layers (Fig. 10). There is no correlation between temperature gradient and the orientation of the densified kernel.

2. There is no evidence of amoeba with WAR kernels containing more than 15% carbide, with the remainder as oxide. However, WAR UO_2 kernels have been observed (Fig. 12) to migrate up the temperature gradient, just as the dense oxide kernels described earlier. As indicated earlier, WAR kernels containing a carbide phase of more than 15% UC_2 tend to be attached to the coating layers on one side of the particle, but there is no correlation with temperature gradient, so this cannot be classified as amoeba. There may be some temptation by the reader to compare the appearance of the WAR particles (Figs. 10 and 11) with the UO_2 kernel (Fig. 1); however, it is emphasized that the operating temperature for the UO_2 kernel was only about 950°C compared to temperatures of about 1350°C for the WAR kernels. At these modest temperatures UO_2 performs well, but neither UO_2 or mixed oxide perform well in the 1350°C range (Fig. 5).

3. Some phase segregation is associated with WAR kernels containing 85% oxide (15% carbide) under irradiation (Figs. 13 and 14). So far this phase segregation has been observed only in the WAR 85% UO_2 fuel.

4. There is considerable fission product attack on the silicon carbide coatings by fission products La, Ce, Pr, and Nd in WAR UC_2 fuels. This same type of attack has been observed in dense UC_2 fuels, irradiated in HRB capsules under accelerated conditions, and also in the Peach Bottom Reactor under real-time conditions. The presence of UO_2 reduces the fission product attack of the silicon carbide layer, apparently by the formation of stable rare earth oxides, which are

Table 3. Summary of ORNL Experimental Data on Irradiated Weak-Acid-Resin-Derived Recycle Fuel

Fissile particle batch No.	Number of particles irradiated	Sample identification	Fast fluence E > 0.18 MeV (n/cm^2)	Burnup (% FIMA)	Resin	Conversion[a] (%)	Design[b] A/B/C/D/E (μm)	Density[b] A/B/C/D/E (g/cm^3)	Maximum fuel[c] temperature (°C)
					HRB-5[(1)]				
52A	5750	1A	3.4×10^{21}	13	IRC-72	95	350/40/30/30/30	6/1.1/1.9/3.18/1.85	1250
	5840	1B	4.0	14					
	5900	1C	4.5	16					
	2950	3A	4.2	15					
	2950	3B	3.9	14					
	2950	3C	3.6	13					
	2950	3D	3.2	12					
					HRB-4[(1)]				
52A	5750	1A	7.8	24	IRC-72	95	350/40/30/30/30	6/1.1/1.9/3.18/1.85	1250
	5840	1B	9.2	27					
	5900	1C	10.3	29					
	2950	3A	9.6	27					
	2950	3B	8.9	25					
	2950	3C	8.1	23					
	2950	3D	7.2	20					
					HRB-6[(2)]				
Pu-295B	28	1C4	7.7	84	IRC-72	?	400/35/25/30/25	3.2/1.2/1.95/3.18/1.95	1250
Pu-296	25	1C5	7.7	84	IRC-72	95	400/35/25/30/25	3.8/1.2/1.95/3.18/1.95	
Pu-297	22	1C6	7.7	84	IRC-72	95	400/35/25/30/25	3.7/1.2/1.95/3.18/1.95	
					HRB-7[(3)]				
OR-2115H	402	13	5.9	80.0	IRC-72	14	400/40/30/30/40	3.2/1.2/1.95/3.18/1.95	1500
OR-2121H	407	14	5.6	79.9	IRC-72	92	300/75/30/30/40	5.3/1.2/1.95/3.18/1.95	
OR-2115H	476	15	5.3	79.9	IRC-72	14	400/40/100	3.2/1.2/1.95	
OR-2121H	511	16	4.9	79.9	IRC-72	92	300/75/85	5.3/1.2/1.95	
					HRB-8[(3)]				
OR-2121H	402	13	7.7	80.4	IRC-72	14	400/40/30/30/40	3.2/1.2/1.95/3.18/1.95	1250
OR-2115H	407	14	7.4	80.3	IRC-72	92	300/75/30/30/40	5.3/1.2/1.95/3.18/1.95	
OR-2121H	476	15	6.9	80.3	IRC-72	14	400/40/100	3.2/1.2/1.95	
OR-2115H	511	16	6.4	80.3	IRC-72	92	300/75/85	5.3/1.2/1.95	
					HRB-9[(4)]				
OR-2208H	593	1	4.7	79.1	IRC-72	100	360/50/30/30/40	3.0/1.2/1.95/3.18/1.95	1250
OR-2121H	433	3	5.8	79.5		100	300/75/30/30/40	5.3/1.2/1.95/3.18/1.95	
OR-2218H	486	4	6.3	79.4		0	360/50/30/30/40	3.7/1.2/1.95/3.18/2.00	
OR-2208H	490	5	6.8	79.9		100	360/50/30/30/40	3.0/1.2/1.95/3.18/1.95	
OR-2115H	373	8	7.8	80.1		15	400/40/30/30/40	3.2/1.2/1.95/3.18/1.95	
OR-2207H	486	9	7.9	80.1		75	360/50/30/30/40	3.0/1.2/1.95/3.18/1.95	
OR-2207H	486	10	7.9	80.1		75	360/50/30/30/40	3.0/1.2/1.95/3.18/1.95	
OR-2208H	469	11	7.9	80.1		100	360/50/30/30/40	3.0/1.2/1.95/3.13/1.95	
OR-2218H	423	12	7.8	80.1		0	360/50/30/30/40	3.7/1.2/1.95/3.18/2.00	
OR-2211H	520	13	7.6	80.0		50	360/50/30/30/40	3.1/1.2/1.95/3.18/2.00	
OR-2121H	398	14	7.2	79.9		100	300/75/30/30/40	5.3/1.2/1.95/3.18/1.95	
OR-2207H	510	15	6.8	79.9		75	360/50/30/30/40	3.0/1.2/1.95/3.18/1.95	
OR-2115H	427	16	6.3	80.0		15	400/40/30/30/40	3.2/1.2/1.95/3.18/1.95	
OR-2211H	566	17	5.8	79.5		50	360/50/30/30/40	3.1/1.2/1.95/3.18/2.00	
OR-2219H	584	18	5.3	79.3		NA	360/50/30/30/40	3.0/1.2/1.95/3.18/2.00	
OR-2207H	616	19	4.7	79.1		75	360/50/30/30/40	3.0/1.2/1.95/3.18/1.95	
OR-2219H	484	6	7.2	80.0		NA	360/50/30/30/40	3.0/1.2/1.95/3.18/2.00	
					HRB-10[(4)]				
OR-2208H	593	1	3.0	77.3	IRC-72	100	360/50/30/30/40	3.0/1.2/1.95/3.18/1.95	1500
OR-2121H	433	3	3.7	78.5		100	300/75/30/30/40	5.3/1.2/1.95/3.18/1.95	
OR-2218H	486	4	4.0	79.2		0	360/50/30/30/40	3.7/1.2/1.95/3.18/2.00	
OR-2208H	490	5	4.3	79.2		100	360/50/30/30/40	3.0/1.2/1.95/3.18/1.95	
OR-2115H	373	8	4.9	79.5		15	400/40/30/30/40	3.2/1.2/1.95/3.18/1.95	
OR-2207H	486	9	5.0	79.6		75	360/50/30/30/40	3.0/1.2/1.95/3.18/1.95	
OR-2207H	486	10	5.0	79.6		75	360/50/30/30/40	3.0/1.2/1.95/3.18/1.95	
OR-2208H	469	11	5.0	79.6		100	360/50/30/30/40	3.0/1.2/1.95/3.18/1.95	
OR-2218H	423	12	4.9	79.5		0	360/50/30/30/40	3.7/1.2/1.95/3.18/2.00	
OR-2211H	520	13	4.8	79.4		50	360/50/30/30/40	3.1/1.2/1.95/3.18/2.00	
OR-2121H	398	14	4.6	79.3		100	300/75/30/30/40	5.3/1.2/1.95/3.18/1.95	
OR-2207H	510	15	4.3	79.2		75	360/50/30/30/40	3.0/1.2/1.95/3.18/1.95	
OR-2115H	427	16	4.0	79.2		15	400/40/30/30/40	3.2/1.2/1.95/3.18/1.95	
OR-2211H	566	17	3.7	78.5		50	360/50/30/30/40	3.1/1.2/1.95/3.18/2.00	
OR-2219H	584	18	3.3	78.0		NA	360/50/30/30/40	3.0/1.2/1.95/3.18/2.00	
OR-2207H	616	19	3.0	77.3		75	360/50/30/30/40	3.0/1.2/1.95/3.18/1.95	
OR-2219H	484	6	4.6	79.3		NA	360/50/30/30/40	3.0/1.2/1.95/3.18/2.00	
					OF-2 (Cell 2)[(4)]				
A-611[d]	4450	A-1-1	e	f	IRC-72	15	360/50/35/30/35	3.0/1.1/1.7/>3.18/1.7	1150
A-601[d]	4440	-2	e	f		75	360/50/35/30/35	3.0/1.1/1.7/>3.18/1.7	
A-611[d]	2530	-3	e	f		15	360/50/35/30/35	3.0/1.1/1.7/>3.18/1.7	
A-611[d]	2530	-4	e	f		15	360/50/35/30/35	3.0/1.1/1.7/>3.18/1.7	
A-601[d]	1980	-5	e	f		75	360/50/35/30/35	3.0/1.1/1.7/>3.18/1.7	
A-601[d]	1980	-6	e	f		75	360/50/35/30/35	3.0/1.1/1.7/>3.18/1.7	
A-611[d]	4450	A-2-1	e	f		15	360/50/35/30/35	3.0/1.1/1.7/>3.18/1.7	
A-611[d]	4450	-2	e	f		15	360/50/35/30/35	3.0/1.1/1.7/>3.18/1.7	
A-601[d]	2520	-3	e	f		75	360/50/35/50/35	3.0/1.1/1.7/>3.18/1.7	
A-601[d]	2520	-4	e	f		75	360/50/35/50/35	3.0/1.1/1.7/>3.18/1.7	
A-611[d]	1980	-5	e	f		15	360/50/35/50/35	3.0/1.1/1.7/>3.18/1.7	
A-601[d]	1980	-6	e	f		75	360/50/35/50/35	3.0/1.1/1.7/>3.18/1.7	

Table 3. (Continued)

Fissile particle batch No.	Number of particles irradiated	Sample identification	Fast fluence E > 0.18 MeV (n/cm^2)	Burnup (% FIMA)	Resin	Conversion[a] (%)	Design[b] A/B/C/D/E (μm)	Density[b] A/B/C/D/E (g/cm^3)	Maximum fuel[c] temperature (°C)
OR-2329H	1920	A-3-2	e	f	IRC-72	0	375/20/35/30/35	3.2/<1.3/1.95/>3.18/2.0	1150
OR-2329H	1920	A-3-4	e	f		0	375/20/35/30/35	3.2/<1.3/1.95/>3.18/2.0	
OR-2322H	1080	A-3-5	e	f		15	360/50/35/30/35	3.1/<1.3/1.95/>3.18/2.0	
OR-2211H	1100	A-3-6	e	f		50	375/50/35/30/35	3.2/<1.3/1.95/>3.18/2.0	
OR-2208H	1040	A-3-7	e	f		100	360/50/35/30/35	3.0/<1.3/1.95/>3.18/2.0	
OR-2322H	850	A-3-9	e	f		15	375/50/35/30/35	3.2/<1.3/1.95/>3.18/2.0	
OR-2329H	850	A-3-10	e	f		0	375/20/35/30/35	3.2/<1.3/1.95/>3.18/2.0	
OR-2208H	820	A-3-11	e	f		100	360/50/35/30/35	3.0/<1.3/1.95/>3.18/2.0	
OR-2121H	1520	A-4-1	e	f	IRC-72	100	320/75/35/30/35	5.0/<1.3/1.95/>3.18/2.0	
OR-2332H	1940	A-4-2	e	f		0	375/50/35/30/35	3.2/<1.3/1.95/>3.18/2.0	
OR-2121H	1520	A-4-3	e	f		100	320/75/35/30/35	5.0/<1.3/1.95/>3.18/2.0	
OR-2332H	1940	A-4-4	e	f		0	375/50/35/30/35	3.2/<1.3/1.95/>3.18/2.0	
OR-2218H	960	A-4-5	e	f		0	360/50/35/30/35	3.7/<1.3/1.95/>3.18/2.0	
OR-2320H	1100	A-4-6	e	f		25	375/50/35/30/35	3.2/<1.3/1.95/>3.18/2.0	
OR-2207H	1080	A-4-7	e	f		75	360/50/35/30/35	3.0/<1.3/1.95/>3.18/2.0	
OR-2218H	750	A-4-9	e	f		0	360/50/35/30/35	3.7/<1.3/1.95/>3.18/2.0	
OR-2332H	860	A-4-10	e	f		0	375/50/35/30/35	3.2/<1.3/1.95/>3.18/2.0	
OR-2207H	850	A-4-11	e	f		75	360/50/35/30/35	3.0/<1.3/1.95/>3.18/2.0	
A-601[d]	1520	B-1-1	e	f	IRC-72	75	360/50/35/30/35	3.0/1.1/1.8/>3.18/1.8	1350
A-601[d]	1520	B-1-2	e	f		75			
A-601[d]	1290	B-1-3	e	f		75			
A-611[d]	1290	B-1-4	e	f		15			
A-611[d]	1290	B-1-5	e	f		15			
A-611[d]	1290	B-1-6	e	f		15			
A-601[d]	1520	B-2-1	e	f		75			
A-611[d]	1520	B-2-2	e	f		15			
A-611[d]	1290	B-2-3	e	f		15			
A-601[d]	1290	B-2-4	e	f		75			
A-601[d]	1290	B-2-5	e	f		75			
A-611[d]	1290	B-2-6	e	f		15			
OR-2329H	660	B-3-2	e	f	IRC-72	0	375/20/35/30/35	3.2/<1.3/1.95/>3.18/2.0	
OR-2322H	650	B-3-3	e	f		15	375/50/35/30/35	3.2/<1.3/1.95/>3.18/2.0	
OR-2211H	660	B-3-4	e	f		50	360/50/35/30/35	3.1/<1.3/1.95/>3.18/2.0	
OR-2208H	530	B-3-5	e	f		100	360/50/35/30/35	3.0/<1.3/1.95/>3.18/2.0	
OR-2329H	560	B-3-7	e	f		0	375/20/35/30/35	3.2/<1.3/1.95/>3.18/2.0	
OR-2322H	550	B-3-8	e	f		15	375/50/35/30/35	3.2/<1.3/1.95/>3.18/2.0	
OR-2218H	490	B-3-9	e	f		0	360/50/35/30/35	3.7/<1.3/1.95/>3.18/2.0	
OR-2208H	530	B-3-10	e	f		100	360/50/35/30/35	3.0/<1.3/1.95/>3.18.2.0	
OR-2329H	560	B-3-11	e	f		0	375/20/35/30/35	3.2/<1.3/1.95/>3.18/2.0	
OR-2322H	550	B-3-12	e	f		15	375/50/35/30/35	3.2/<1.3/1.95/>3.18/2.0	
OR-2332H	660	B-4-2	e	f	IRC-72	0	375/50/35/30/35	3.2/<1.3/1.95/>3.18/2.0	
OR-2218H	580	B-4-3	e	f		0	360/50/35/30/35	3.7/<1.3/1.95/>3.18/2.0	
OR-2320H	660	B-4-4	e	f		25	375/50/35/30/35	3.2/<1.3/1.95/>3.18/2.0	
OR-2207H	550	B-4-5	e	f		75	320/75/35/30/35	5.0/<1.3/1.95/>3.18/2.0	
OR-2121H	440	B-4-6	e	f		100	320/75/35/30/35	5.0/<1.3/1.95/>3.18/2.0	
OR-2332H	560	B-4-7	e	f		0	375/50/35/30/35	3.2/<1.3/1.95/>3.18/2.0	
OR-2218H	490	B-4-8	e	f		0	360/50/35/30/35	3.7/<1.3/1.95/>3.18/2.0	
OR-2320H	560	B-4-9	e	f		25	375/50/35/30/35	3.2/<1.3/1.95/>3.18/2.0	
OR-2207H	550	B-4-10	e	f		75	320/75/35/30/35	5.0/<1.3/1.95/>3.18/2.0	
OR-2332H	560	B-4-11	e	f		0	375/50/35/30/35	3.2/<1.3/1.95/>3.18/2.0	
					OF-2 (Cell 1)[4]				
A-601[d]	2500	C-1-1	e	f	IRC-72	75	360/50/35/30/35	3.1/1.1/1.8/>3.18/1.8	
A-601[d]	2500	C-1-2	e	f		75			
A-611[d]	2970	C-1-3	e	f		15			
A-601[d]	6790	C-1-4	e	f		75			
A-615[g]	2440	C-2-1	e	f		75			
A-601[d]	2500	C-2-2	e	f		75			
A-615[g]	2900	C-2-3	e	f		75			
A-615[g]	6648	C-2-4	e	f		75			
A-611[d]	2500	C-3-1	e	f		15			
A-611[d]	2500	C-3-2	e	f		15			
A-601[d]	2960	C-3-3	e	f		75			
A-611[d]	6800	C-3-4	e	f		15			
A-615[g]	2440	C-4-1	e	f		75			
A-611[d]	2500	C-4-2	e	f		15			
A-601[d]	2960	C-4-3	e	f		75			
A-601[d]	6790	C-4-4	e	f		75			

[a]Percent conversion = $\frac{2-x}{2} \cdot 100$, where x = atomic fraction of oxygen in kernel; e.g., $UCyO_{0.5}$ = 75% converted.

[b]A = kernel; B = buffer; C = IPyC; D = SiC; E = OPyC.

[c]Maximum fuel design temperature.

[d]12.7 cm (5 in.) diam frit.

[e]Peak fast fluence will be 8×10^{21} n/cm^2 at end of irradiation period.

[f]Peak burnup will be 80% FIMA at end of irradiation period.

[g]12.7 cm (5 in.) diam cone.

[1]F. J. Homan et al., *Irradiation Performance of HTGR Fuel Rods in HFIR Experiments HRB-4 and -5*, ORNL-5115, in publication.

[2]F. J. Homan et al., *Irradiation Performance of HTGR Fuel Rods in HFIR Experiment HRB-6*, ORNL-TM-5011 (December 1975).

[3]K. H. Valentine et al., *Irradiation Performance of HTGR Fuel Rods in HFIR Experiments HRB-7 and -8*, in preparation.

[4]*HTGR Base Technology Program Annu. Progr. Rep. Jan. 1, 1974 through June 30, 1975*, Sect. 6.5.3, in preparation.

Table 3a. Results of Irradiation Tests on Weak-Acid-Resin-Derived Recyle Fuel

Sample identification	Remarks[a]	
	HRB-5	
1A, 1B, 1C	Extruded rods; carbonized in covered graphite tray; fine cracks in SiC observed; no amoeba.	
3A, 3B	Slug-injected rods; carbonized in packed Al_2O_3.	Matrix-particle interaction recognized as a potential problem with high pitch-coke yields. No amoeba. Kernel densification apparent.
3C, 3D	Slug-injected rods; carbonized in-block.	
	HRB-4	
1A, 1B, 1C	Extruded rods; carbonized in covered graphite tray; fine cracks in SiC observed; no amoeba.	
3A, 3B	Slug-injected rods; carbonized in packed Al_2O_3.	Attack of SiC coating by Pd and rare-earth fission products observed. Phase segregation in about 25% of the kernels. Metallographic results indicate not all particles were 95% converted.
3C, 3D	Slug-injected rods; carbonized in-block.	
	HRB-6	
1C4, 1C5	Loose particles in graphite tube; recovery of all particles not possible; majority failed.	
1C6	Loose particles in graphite tube; tube broke during irradiation; particles lost.	
	HRB-7	
13	Slug-injected rod; no failures (Metallography); buffer consumed; slight attack of SiC by rare earths.	
14	Slug-injected rod; ∿ 50% failed (Metallography); ILTI graphitized by rare earths on cold side.	
15	Slug-injected rod; no failures (Metallography); buffer consumed; phase segregation in kernel; no evidence of rare earth in coatings.	
16	Slug-injected rod; no failures (Metallography); unilateral movement of kernel through buffer; no evidence of rare earth in coatings.	
	HRB-8	
13	Slug-injected rod; no failures (Metallography); buffer consumed; slight attack of SiC by rare earths.	
14	Slug-injected rod; all failed (Metallography); ILTI graphitized by rare earths on cold side.	
15	Slug-injected rod; no failures (Metallography); buffer consumed; phase segregation in kernel; no evidence of rare earth in coatings.	
16	Slug-injected rod; no failures (Metallography); kernel densification apparent; buffer intact; no evidence of rare earth in coatings.	
	HRB-9	
1, 3, 4, 5	Slug-injected rod; stereo-exam only. No broken particles on surface.	
6	Slug-injected rod; ∿ 20% failed (Metallography); buffer in half of particles densified and breached; two-phase kernel; Slight accumulation of rare earths on cold side; no graphitization of ILTI; slight attack of SiC.	
8	Slug-injected rod; no failures (Metallography); buffer consumed; phase segregation in kernel.	
9	Slug-injected rod; no failures (Metallography); buffer intact; phase segregation in kernel; evidence of rare earth accumulation on cold side; no graphitization of ILTI; no attack of SiC	
10	Warm-molded rod; no failures (Metallography); buffer intact; phase segregation in kernel; less evidence of rare earth accumulation in rod 9; no graphitization of ILTI; no attack of SiC.	
11	Slug-injected rod; ∿ 75% failed (Metallography); accumulation of rare earth on cold side; graphitization of ILTI; no attack of SiC; two-phase kernel.	
12	Slug-injected rod; no failures (Metallography); amoeba through buffer; rare earths retained in kernel; slight attack of SiC on hot side (2 μm).	
13	Slug-injected rod; no failures (Metallography); buffer intact but densified around kernel; phase segregation in kernel; accumulation of rare earths on cold side; no graphitization of ILTI; no attack of SiC.	
14	Slug-injected rod; ∿ 50% failed (Metallography); phase segregation in kernel; accumulation of rare earths on cold side; graphitization of ILTI; attack of SiC (∿ 5 μm).	
15	Slug-injected rod; stereo-exam only; no failures.	
16	Slug-injected rod; no failures (Metallography); buffer consumed; phase segregation in kernel.	
17	Slug-injected rod; same remarks as for HRB-9, Rod 13 (50% converted).	
18	Slug-injected rod; stereo-exam only; no broken particles.	
19	Slug-injected rod; stereo-exam only; no broken particles.	
	HRB-10	
1	Slug-injected rod; not examined, due to reaction with thermocouple.	
3	Slug-injected rod; stereo-exam only; no broken particles.	
4, 5	Slug-injected rod; stereo-exam only; no broken particles.	
6	Slug-injected rod; ∿ 30% failed (Metallography); accumulation of rare earths on cold side; graphitization of ILTI and buffer; attack of SiC with complete penetration.	
8	Slug-injected rod; no failures (Metallography); buffer consumed; phase segregation in kernel.	
9	Slug-injected rod; ∿ 8% failed (Metallography); phase segregation in kernel; accumulation of rare earths on cold side. slight graphitization of ILTI; no attack of SiC.	
10	Warm-molded rod; no failures (Metallography); phase segregation in kernel; accumulation of rare earths on cold side; no graphitization of ILTI; slight attack of SiC.	

Table 3a. (Continued)

Sample identification	Remarks[a]
11	Slug-injected rod; ∿ 18% failed (Metallography); two-phase kernel; accumulation of rare earths on cold side; graphitization of ILTI; attack of SiC (∿ 5 μm).
12	Slug-injected rod; ∿ 5% failed (Metallography); amoeba through buffer; rare earths retained in kernel; attack of SiC (slight to complete penetration).
13	Slug-injected rod; no failures (Metallography); same remarks as for HRB-9, Rod 13 (50% converted), except more evidence of rare-earth accumulation.
14	Slug-injected rod; ∿ 30% failures (Metallography); two-phase kernel, accumulation of rare earths on cold side; graphitization of ILTI; attack of SiC (complete penetration).
15	Slug-injected rod; no failures (Metallography); accumulation of rare earths on cold side; slight graphitization of ILTI; no attack of SiC; phase segregation in kernel.
16, 17	Slug-injected rod; stereo-exam only; no broken particles.
18	Slug-injected rod; ∿ 40% failed (Metallography); same remarks as for HRB-10, Rod 6.
19	Slug-injected rod; no failures (Metallography); phase segregation in kernel; no accumulation of rare earths; no graphitization of ILTI; no attack of SiC.
	OF-2 (Cell 2)
A-1-1, -2, -3, -4, -5, -6 A-2-1, -2, -3, -4, -5, -6	All slug-injected rods; initial R/B values for $^{85m}Kr = 7.5 \times 10^{-6}$; After 4200 hr (∿ 1/2 irradiation time) R/B $^{85m}Kr = 1 \times 10^{-5}$. Postirradiation examination scheduled to begin in September 1976.
A-3-2, -4, -5, -6 -7, -9, -10, -11 A-4-1, -2, -3, -4, -5, -6, -7, -9, -10, -11 B-1-1, -2, -3, -4, -5, -6, B-2-1, -2, -3, -4, -5, -6 B-3-2, -3, -4, -5, -7, -8, -9, -10, -11, -12 B-4-2, -3, -4, -5, -6 -7, -8, -9, -10, -11	All slug-injected rods; initial R/B values for $^{85m}Kr = 7.5 \times 10^{-6}$. After 4200 hr (∿ 1/2 irradiation time) R/B $^{85m}Kr = 1 \times 10^{-5}$. Postirradiation examination scheduled to begin in September 1976.
	OF-2 (Cell 1)
C-1-1, -2, -3, -4 C-2-1, -2, -3, -4 C-3-1, -2, -3, -4 C-4-1, -2, -3, -4	All fuel rods fabricated by slug-injection process. Initial ^{85m}Kr R/B values = $< 2 \times 10^{-5}$; After 4200 hr irradiation (∿ 1/2 full scheduled term) ^{85m}Kr R/B value = 7×10^{-5}. Postirradiation examination scheduled to begin in September 1976.

[a]References to "% failed particles" are based on failures observed in metallographic sections, and therefore are not statistically significant since normally < 20 fissile particles are exposed in a random plane-of-polish. These results are, however, indicators of relative performance.

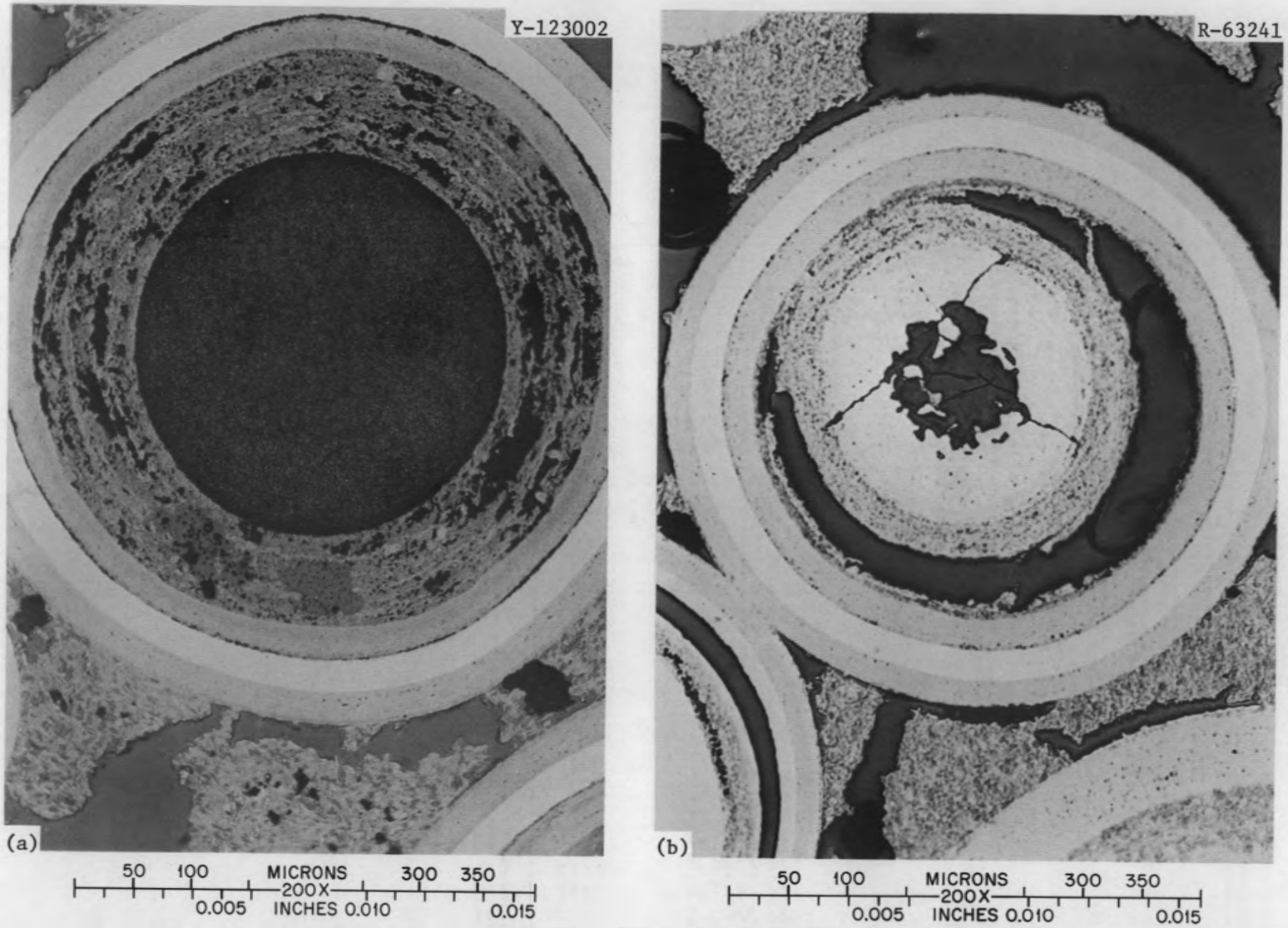

Fig. 10. Weak-Acid Resin Particles Used in Fuel Rods for Irradiation Testing. (a) Unirradiated. (b) Irradiated in HRB-5, rod 3B.

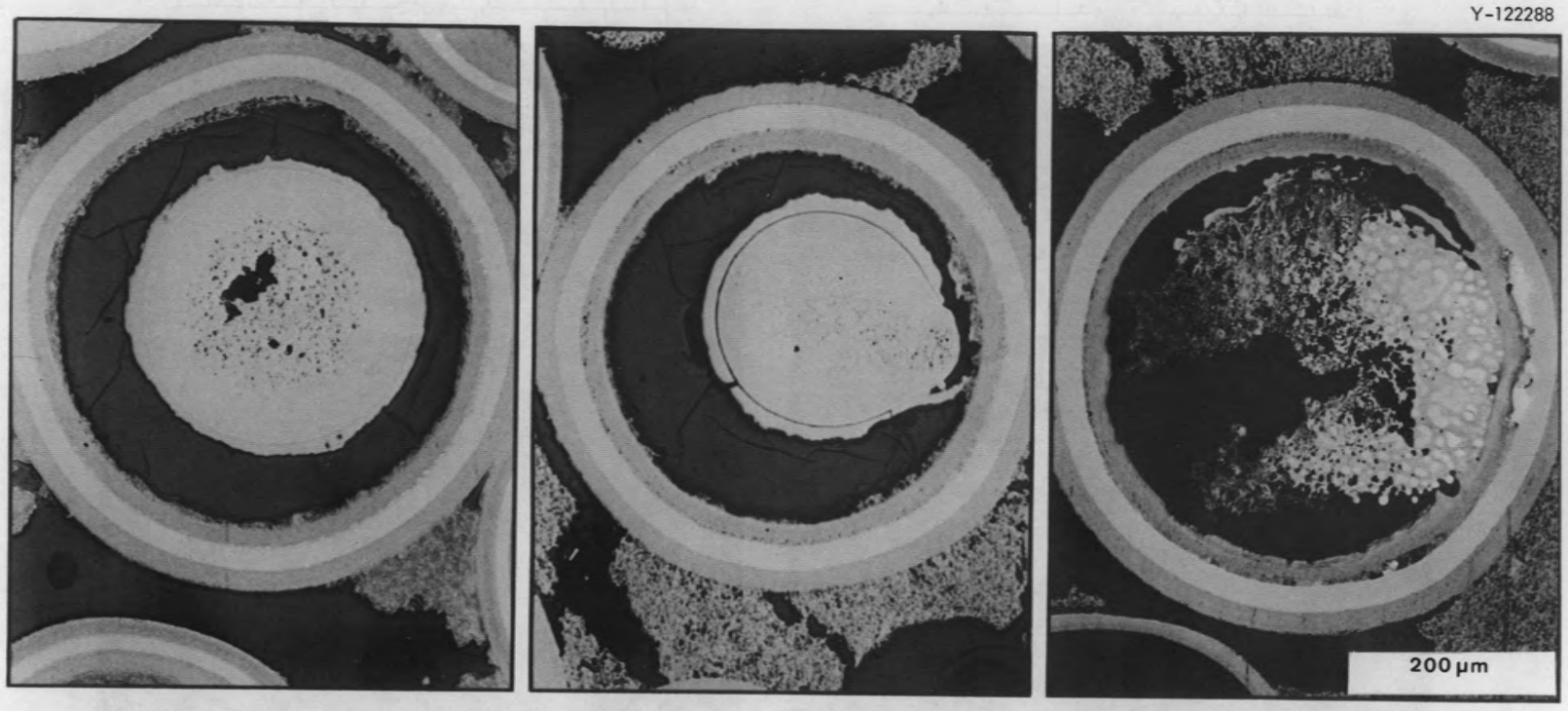

Fig. 11. Appearance of WAR UC_2 Particles From HRB-4 Specimen 3B. Peak operating temperature, 1350°C; burnup, 84% FIMA; fast neutron exposure, 8.9×10^{21} n/cm^2 (>0.18 MeV).

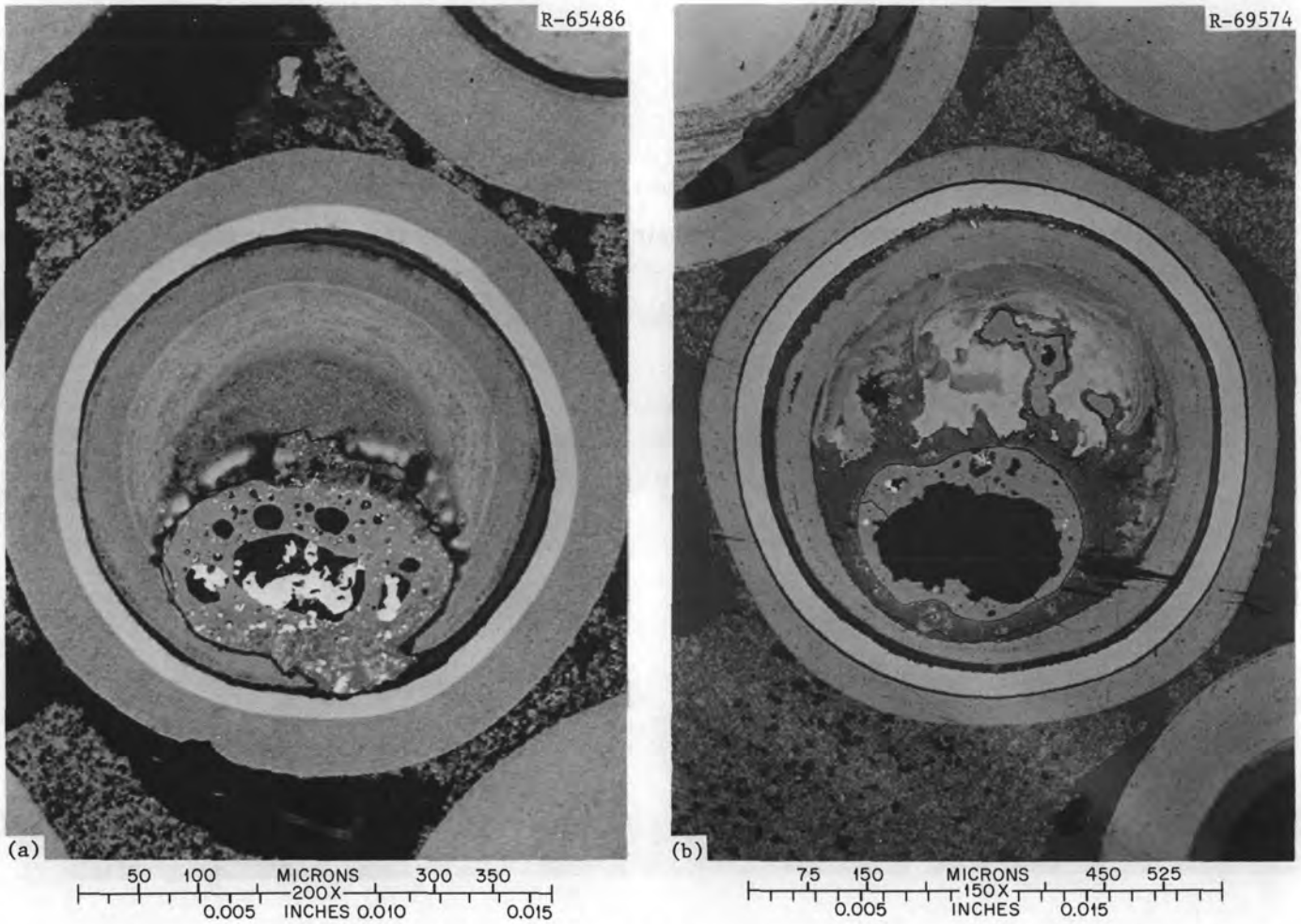

Fig. 12. Triso-Coated (a) Sol-Gel UO_2 Irradiated in Rod 13 of Capsule HRB-10 to 80% FIMA at 1300°C in a Temperature Gradient of 500°C/cm. (b) Weak-acid-resin-derived UO_2 irradiated in rod 7 of HRB-7 to 80% FIMA at 1260°C in a temperature gradient of 700°C/cm. Both particles were located near the surface of the fuel rods and experienced steep temperature gradients during irradiation. Note that the performance of the dense (about 10 g/cm^3) sol-gel kernels is about the same as the porous (about 3 g/cm^3) WAR kernels under very similar irradiation conditions. Both kernels experienced severe migration toward the hot side of the particle.

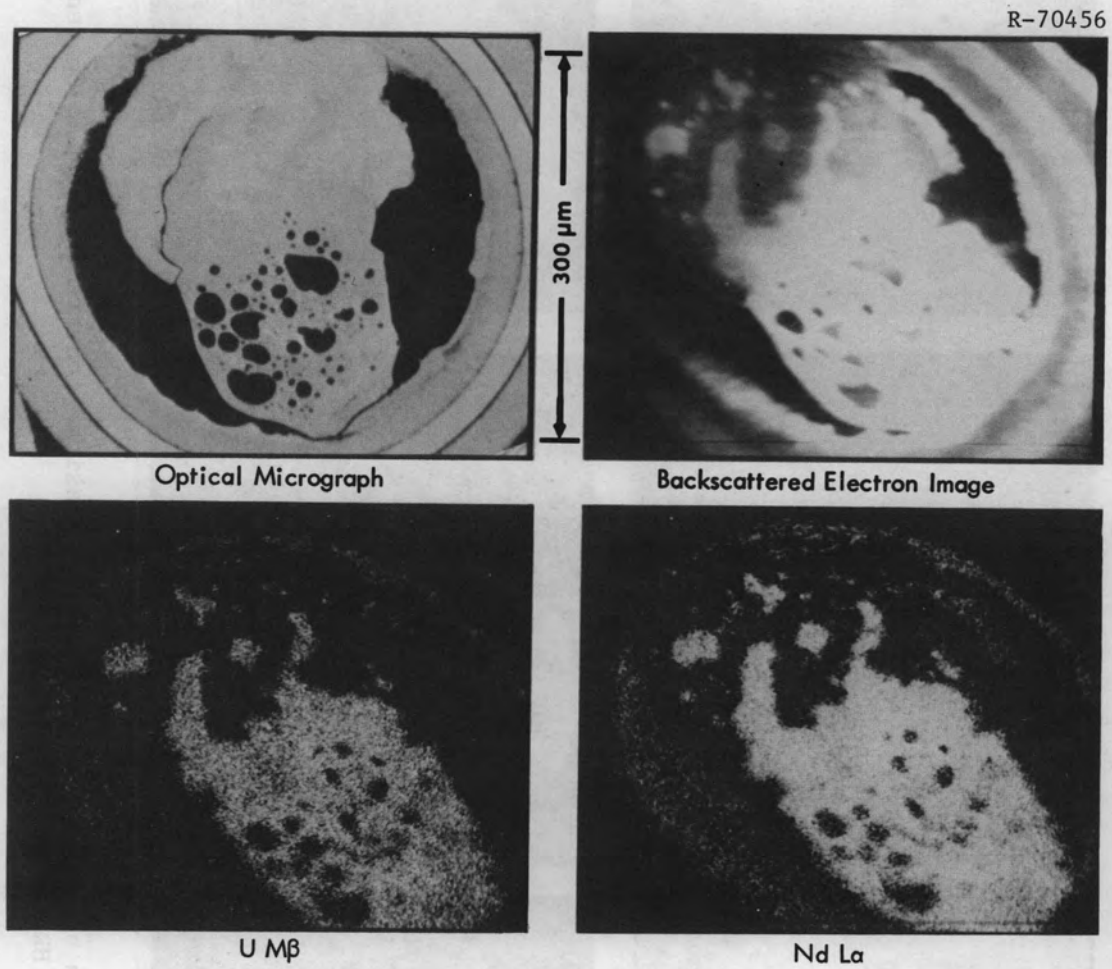

Fig. 13. Distribution of Uranium and Rare-Earth Fission Products (Represented by Neodymium X-Ray Display) in a 15%-Converted Weak-Acid-Resin-Derived Particle. There is no indication that the neodymium penetrated the inner pyrocarbon layer. The neodymium display is representative of cerium, praseodymium, and lanthanum.

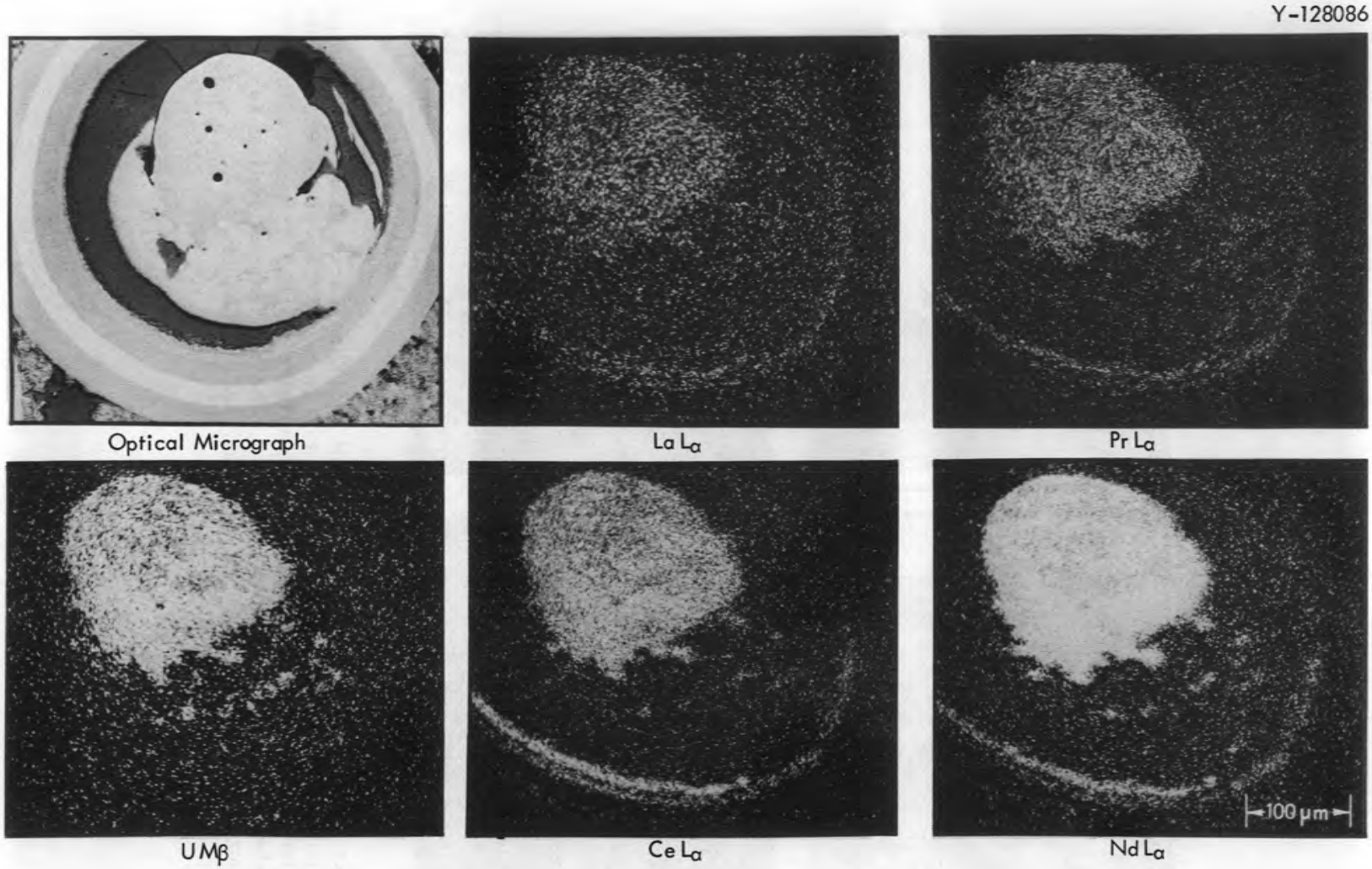

Fig. 14. Distribution of Uranium and Rare-Earth Fission Products in a Triso-Coated 15%-Reduced WAR Particle Irradiated in HRB-8.

retained in the kernel. Optical metallography and shielded microprobe displays of fuel irradiated in the HRB-4 capsule are shown in Fig. 15. This fuel was nominally 95% UC_2. A similar display for reference fresh fissile fuel (UC_2) irradiated under real-time conditions in the Peach Bottom Reactor is shown in Fig. 16. It is emphasized that the UC_2 shown in Fig. 16 has been irradiated to less than 20% full burnup and fast-neutron exposure expected for the large HTGR.[19] Both WAR UC_2 and dense UC_2 performed similarly in fuel irradiated in HRB-7 (Fig. 17). The polarized light portion of this figure reveals the areas of fission product attack as bright areas, indicating a high degree of optical activity.

5. There is a considerable temperature gradient effect on the fission product attack discussed above. Under high-temperature gradients the fission products are concentrated on the cold side of the particle, and failure of the silicon carbide layer is likely, as shown on the left side of Fig. 18. Under less severe temperature gradients, the fission products are less concentrated and do less damage. The particle shown on the right side of Fig. 18 operated at the center of the same fuel rod as the particle on the left. The temperature gradient is zero at the center of the rod, and even though the operating temperature was higher, less damage was done to the coatings by the fission products. The bottom portion of the figure, in polarized light, shows the fission products as light regions. The temperature gradient of 1000°C/cm is about 30% higher than the maximum temperature gradient shown for a large HTGR in Table 1.

Fission product attack of the coatings appears to be the limiting performance feature of WAR UC_2 fuels. Thermal migration appears to be limiting for WAR UO_2. Intermediate compositions appear to do well compared with these extremes. In the HRB-7 through -10 experiments, WAR fissile fuels with conversion levels of 0, 15, 50, 75, and 100% were tested (Fig. 19). These WAR kernels had reference Triso* coatings and were fabricated into fuel rods using the slug-injection[20] technique. As indicated earlier, the WAR UO_2 kernel has migrated up the temperature gradient. The WAR UC_2 particle shown has failed from fission product attack of the silicon carbide layer. Figure 20 shows an optical photomicrograph of a WAR UC_2 particle irradiated in HRB-8. Also shown are electron microprobe displays for the rare earth fission products La, Pr, Ce, and Nd. The graphitization of the inner low-temperature isotropic layer and failure of the silicon carbide in the regions occupied by the fission products suggest that fission product interaction with the silicon carbide coating caused the failure.

---

*The reference Triso design calls for four coatings applied to the kernel. The first coating is called the buffer, and is a porous (about 50% dense) layer of pyrolytic carbon. The next coating is called the inner low-temperature isotropic (ILTI) layer, which is dense pyrolytic carbon (about 85% dense). The third layer is silicon carbide of near theoretical density. The fourth layer is the outer low-temperature isotropic (OLTI) layer, which is similar to the ILTI. These layers are applied to retain fission products.

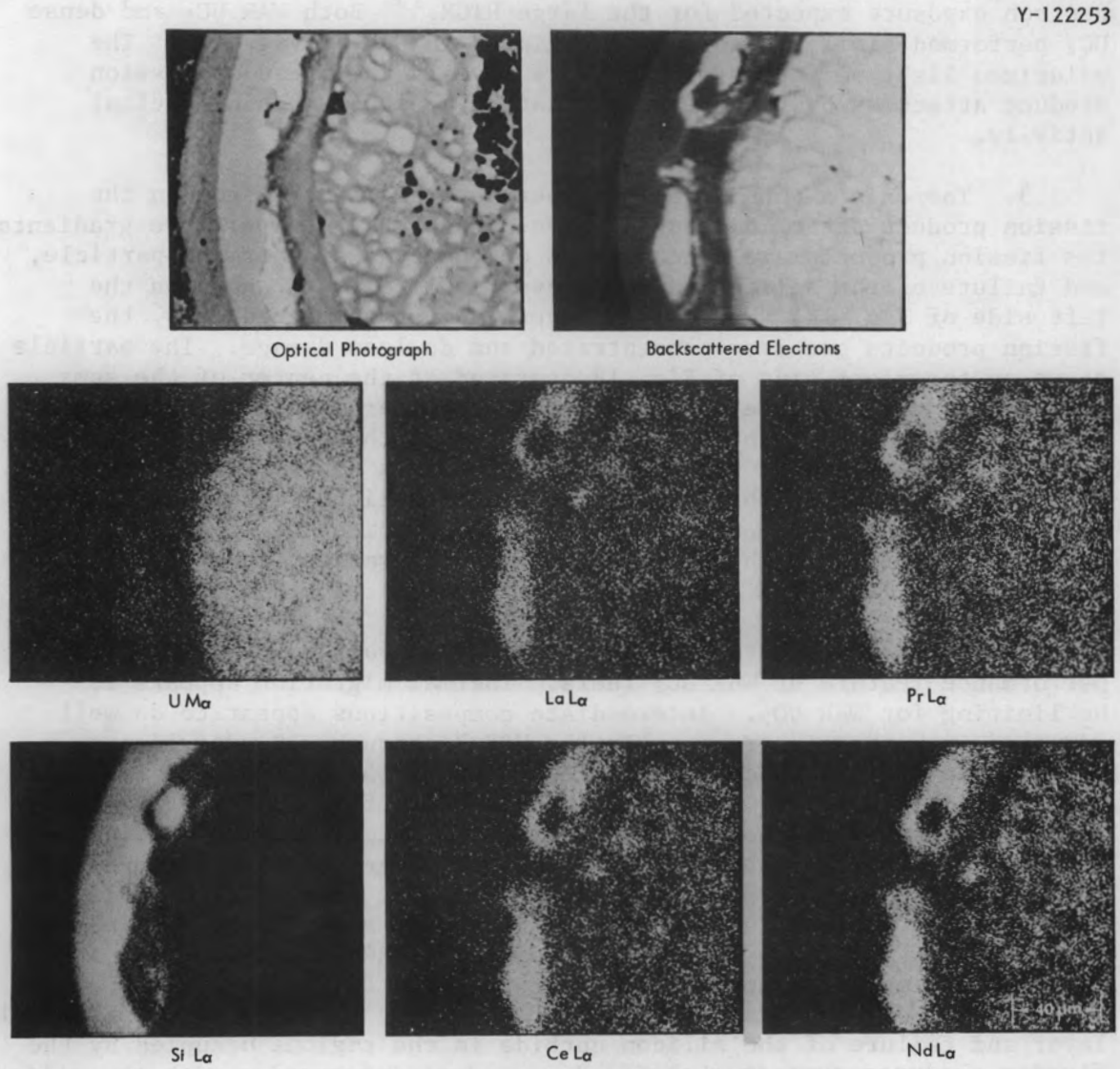

Fig. 15. Weak-Acid-Resin UC_2 Particle from Capsule HRB-4. Peak operating temperature, about 1350°C; burnup, about 84% FIMA; fast neutron exposure, about 8.9×10^{21} n/cm^2 (>0.18 MeV).

Y-123799

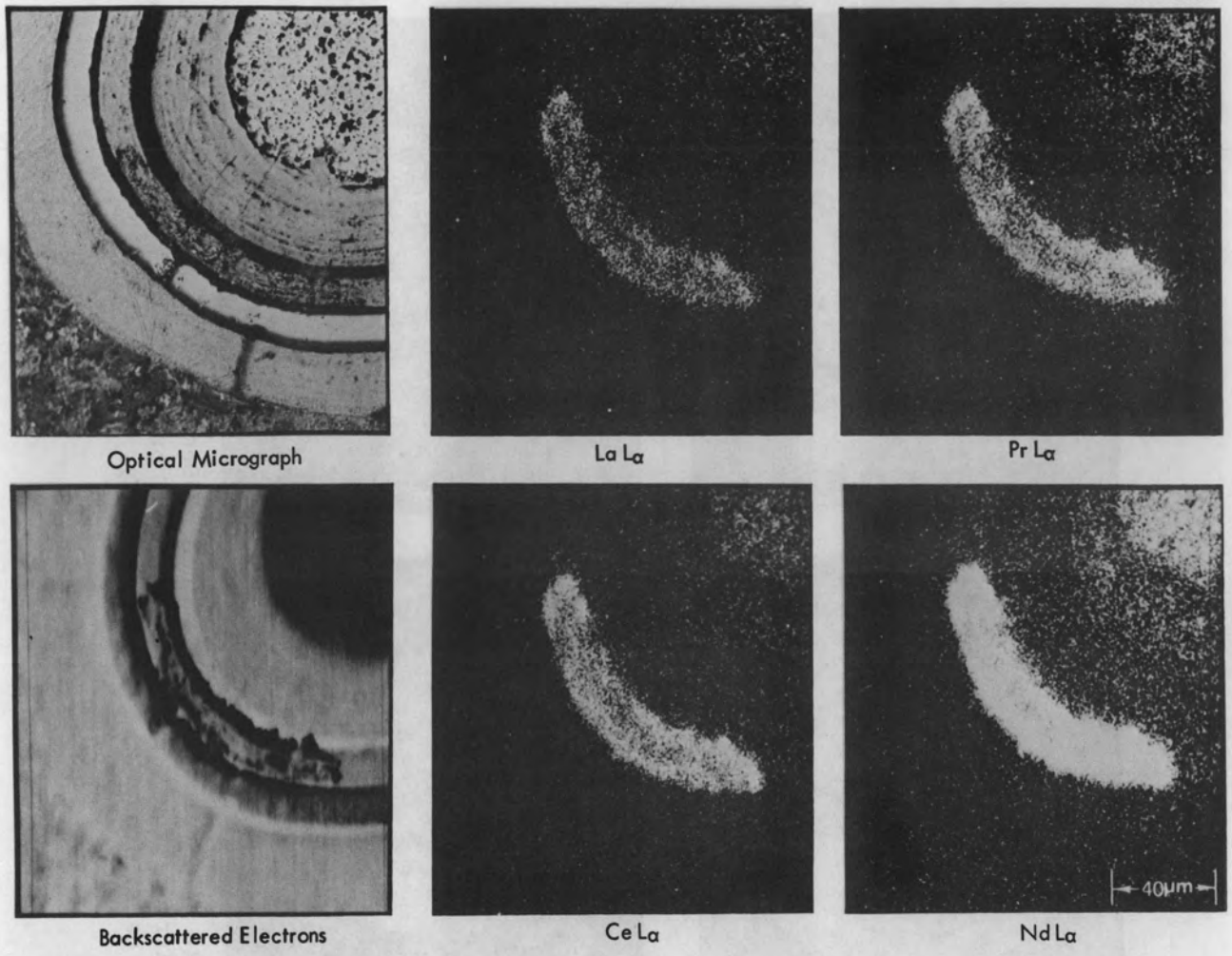

Fig. 16. Rare-Earth Fission Product Attack of Coating Layers has Caused Failure of This Triso-Coated Dense UC_2 Particle from RTE-4. This particle was irradiated in the Peach Bottom Reactor to less than 20% of the burnup and neutron exposure anticipated in a commercial HTGR at an irradiation temperature of less than 1200°C.

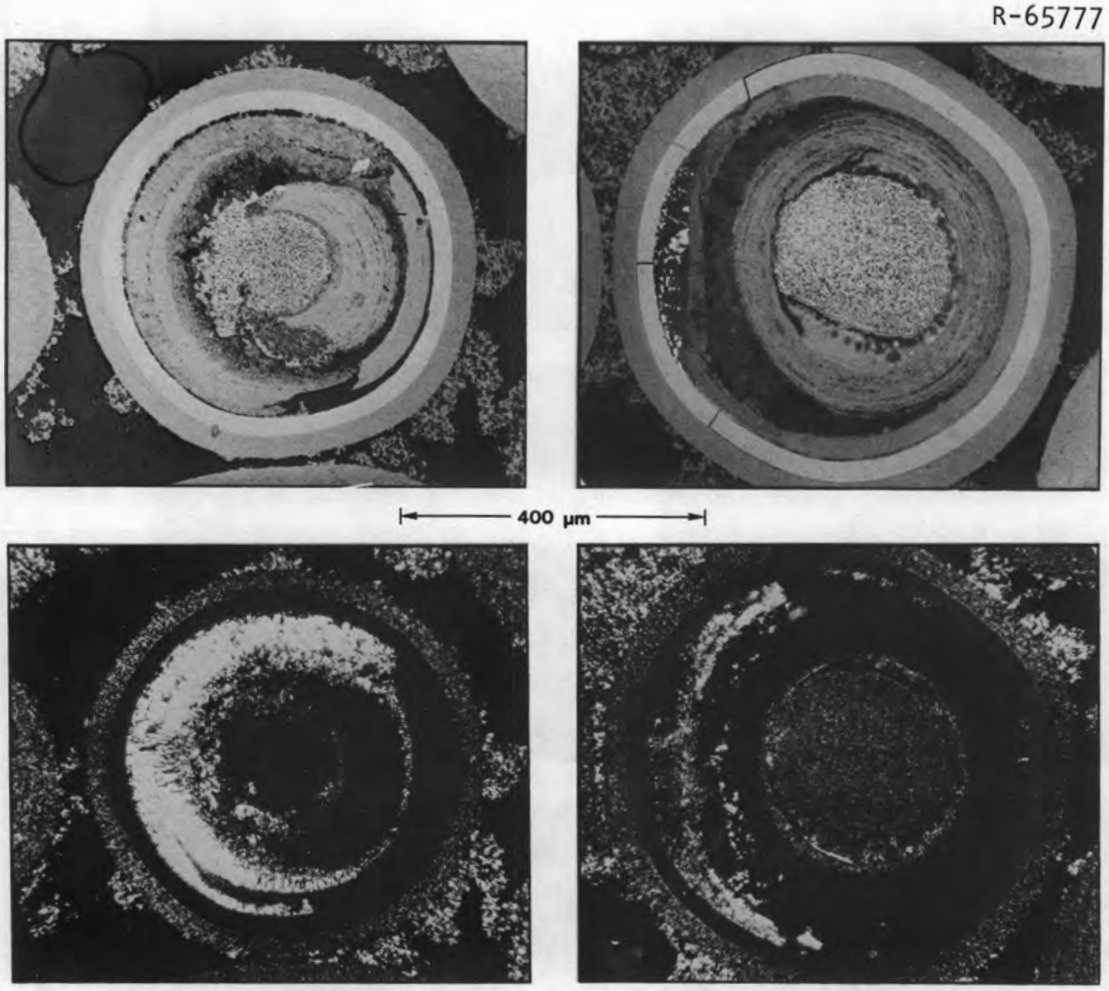

Fig. 17. Relative Performance of Dense Melted (VSM) UC_2 and WAR UC_2 in Irradiation Capsule HRB-7. Top: bright field. Bottom: polarized light. Left: dense UC_2. Right: WAR UC_2.

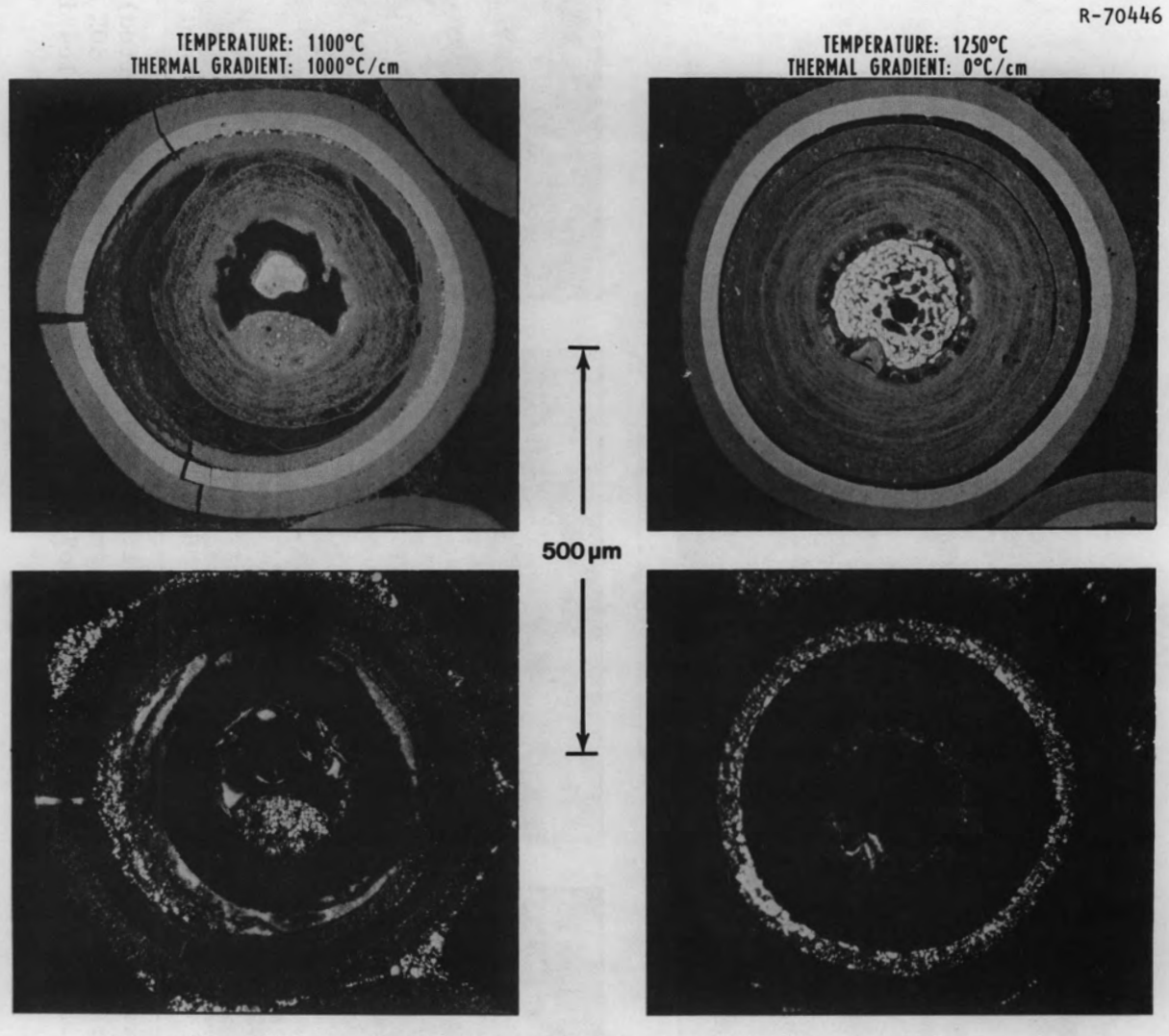

Fig. 18. Effect of Thermal Gradient on Distribution of Rare-Earth Fission Products in a Triso-Coated 100%-Converted WAR UC_2 Kernel. Top: bright field. Bottom: polarized light.

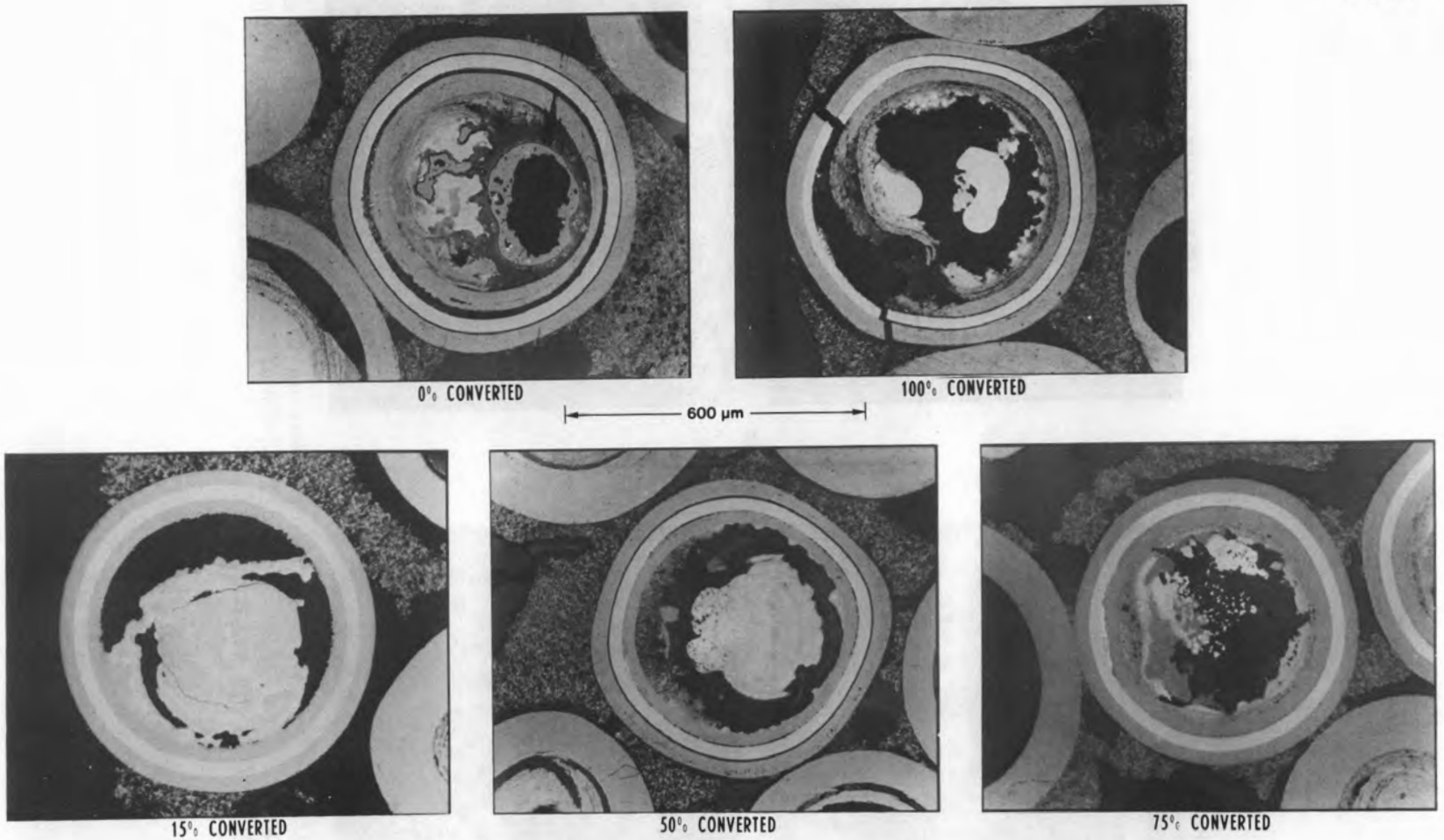

Fig. 19. Relative Performance of WAR Kernels Within the Range of UO_2 (0% Converted) to UC_2 (100% Converted). Irradiated at a maximum fuel temperature of 1500°C to a burnup of 80% FIMA. Fast fluence ranged from 4.3 to 5.0×10^{21} n/cm^2 (>0.18 MeV). The hot side of the particles is on the right.

Y-127988

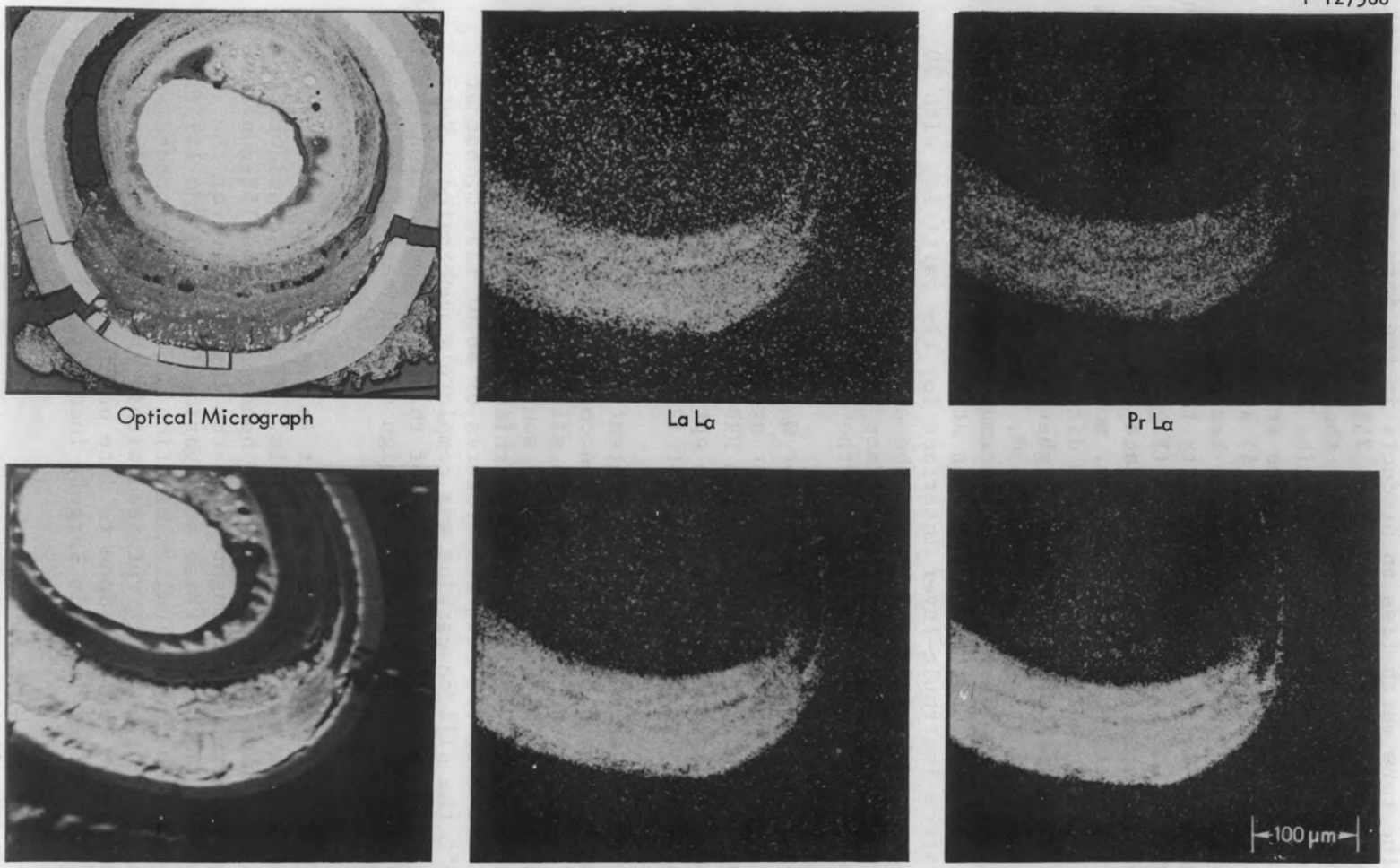

Fig. 20. Electron Microprobe Displays Show the Location of Rare-Earth Fission Products in Triso-Coated Weak-Acid-Resin-Derived UC_2 Fuel Irradiated in Capsule HRB-8 to 85% FIMA at 1130°C and 990°C/cm. Note that rare earths have left the kernel and collected at the inner surface of the SiC layer, causing extensive damage to both the inner LTI and SiC layers.

We calculated (see following section) the amount of UO_2 necessary to retain the rare earth fission products in the form of oxides in WAR fuels irradiated to full burnup (about 75% FIMA*). The irradiation results from HRB-7 through -10 support the conclusions reached in these calculations. The UO_2 fuel retains all the rare earth fission products in the kernel since the oxides are stable (Fig. 21). The 15%-converted WAR fuel (Figs. 13 and 14) also retained most of the rare earth fission products within the kernel. As the amount of UC_2 in the kernel is increased, the capacity to hold the rare earth fission products within the kernel is reduced (Figs. 22 and 23). Neodymium accumulates slightly at the inner surface of the SiC layer for the 50%-converted fuel (Fig. 22). However, most of the neodymium has been retained in the kernel. The neodymium display represents the rare earth fission products. In Fig. 23 higher magnification views of the cold side of coatings for the 15, 50, and 75%-converted fuels shown in Fig. 19 are shown. Slight accumulations of fission products, believed to be rare earths, can be seen at the silicon carbide inner low-temperature isotropic-layer interface for the particles with 50 and 75%-converted kernels. As noted above, the amount of fission product accumulation at the inner surface of the SiC layer increases with the percentage of UC_2 present in the kernel.

The optimum kernel composition for WAR fuels has not yet been determined. Experiments now in-reactor are designed to establish the optimum UO_2 content. The results from HRB-7 through -10, and the thermodynamic calculations, suggest an optimum value of about 35% conversion, with a permissible range of ±20%.

The argument against high UC_2 content is clear. Some problems in addition to amoeba have also been encountered with high UO_2 content. While no fission product attack of the silicon carbide layer was noted with the WAR UO_2 fuel, there was some evidence of oxidation of the inner surface of the silicon carbide layer (Fig. 24). The attack was moderate for fuel temperatures of about 1250°C, but at about 1500°C the silicon carbide was completely penetrated. Very slight oxidation was noted when fuel of this same composition was irradiated in capsule HRB-9 with a design centerline temperature of 1250°C.

From the processing standpoint, it is desirable to maximize the UO_2 content in the two-phase WAR kernels. Therefore, considerable effort has been made to understand the behavior of the 15%-converted fuel, which is currently thought to be the lower limit for the conversion specification. Phase segregation (Figs. 13 and 14) is apparent both from the optical examination and from microprobe work. The uranium-bearing phase is retained within the outer boundary of the buffer layer. The work done to date on 15%-converted fuel indicates that the buffer layer is largely incorporated into the kernel.

---

*FIMA = Fissions per Initial Metal Atom.

Y-129593

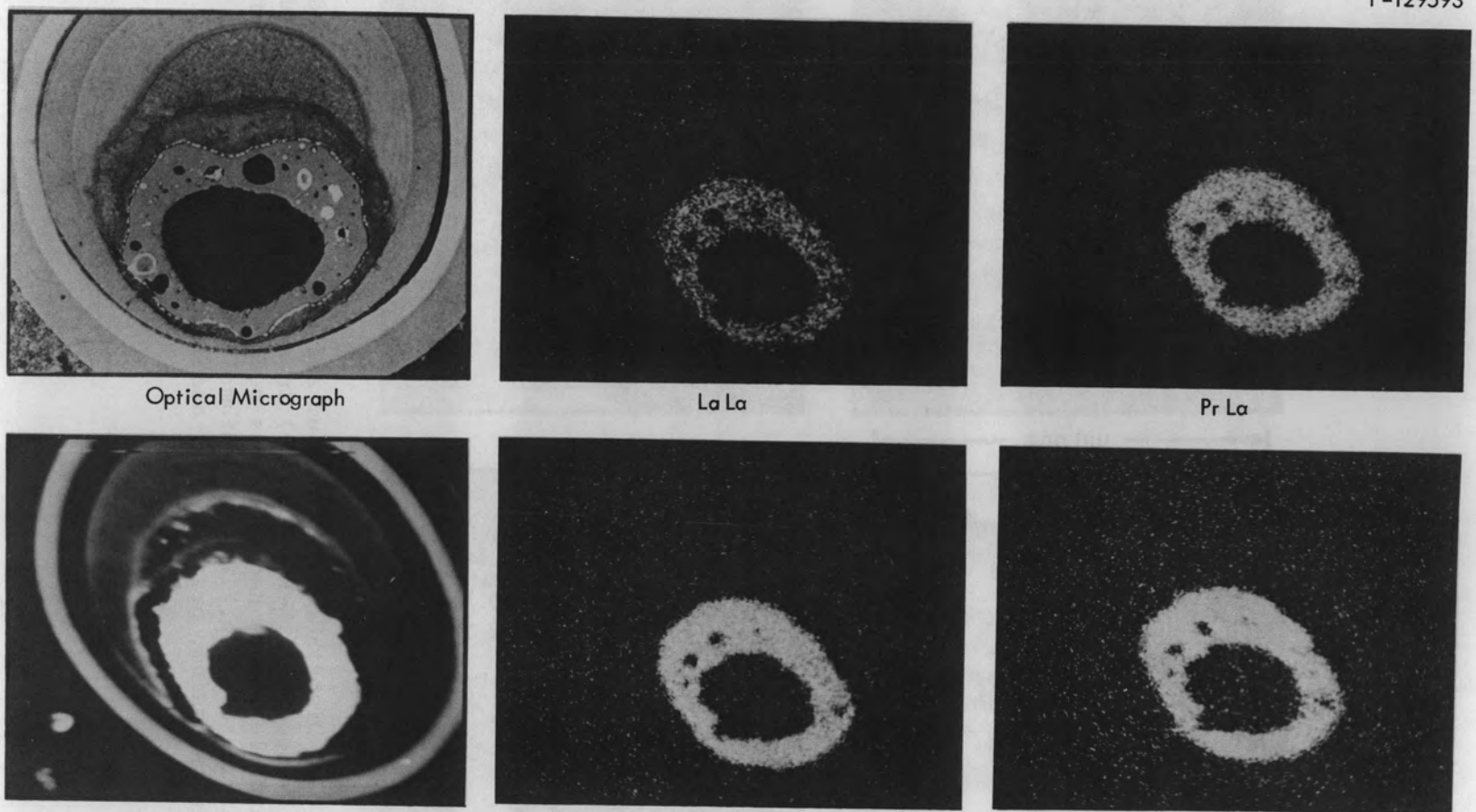

Fig. 21. Retention of Rare-Earth Fission Products in the Kernel of a Sol-Gel UO_2 Triso-Coated Particle Irradiated in HRB-8.

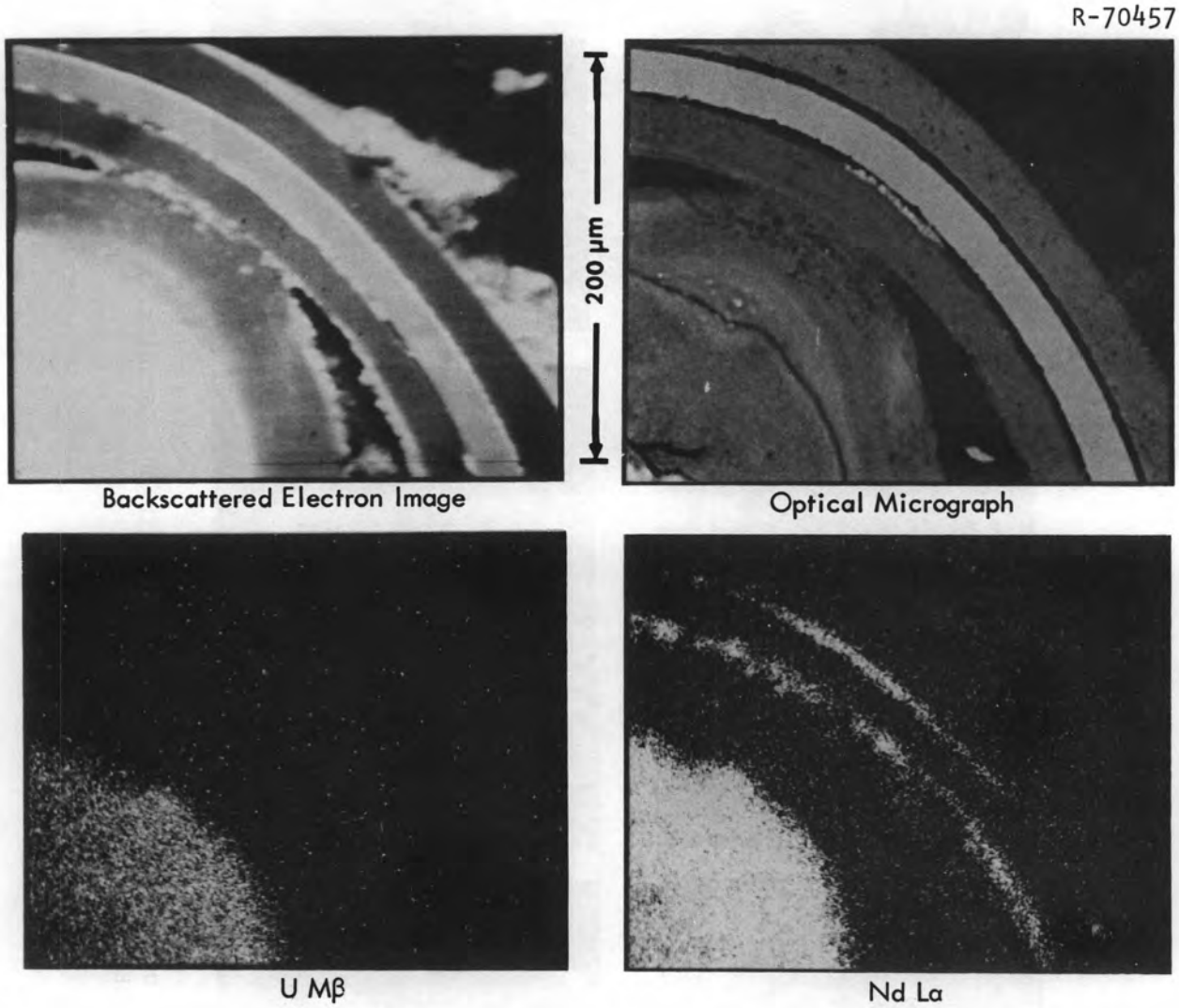

Fig. 22. Distribution of Uranium and Rare-Earth Fission Products (Typified by Neodymium X-Ray Display) in a 50%-Converted Weak-Acid-Resin-Derived Particle. Note neodymium has reached the inner surface of the silicon carbide coating. The neodymium display is representative of the other products cesium, praseodymium, and lanthanum.

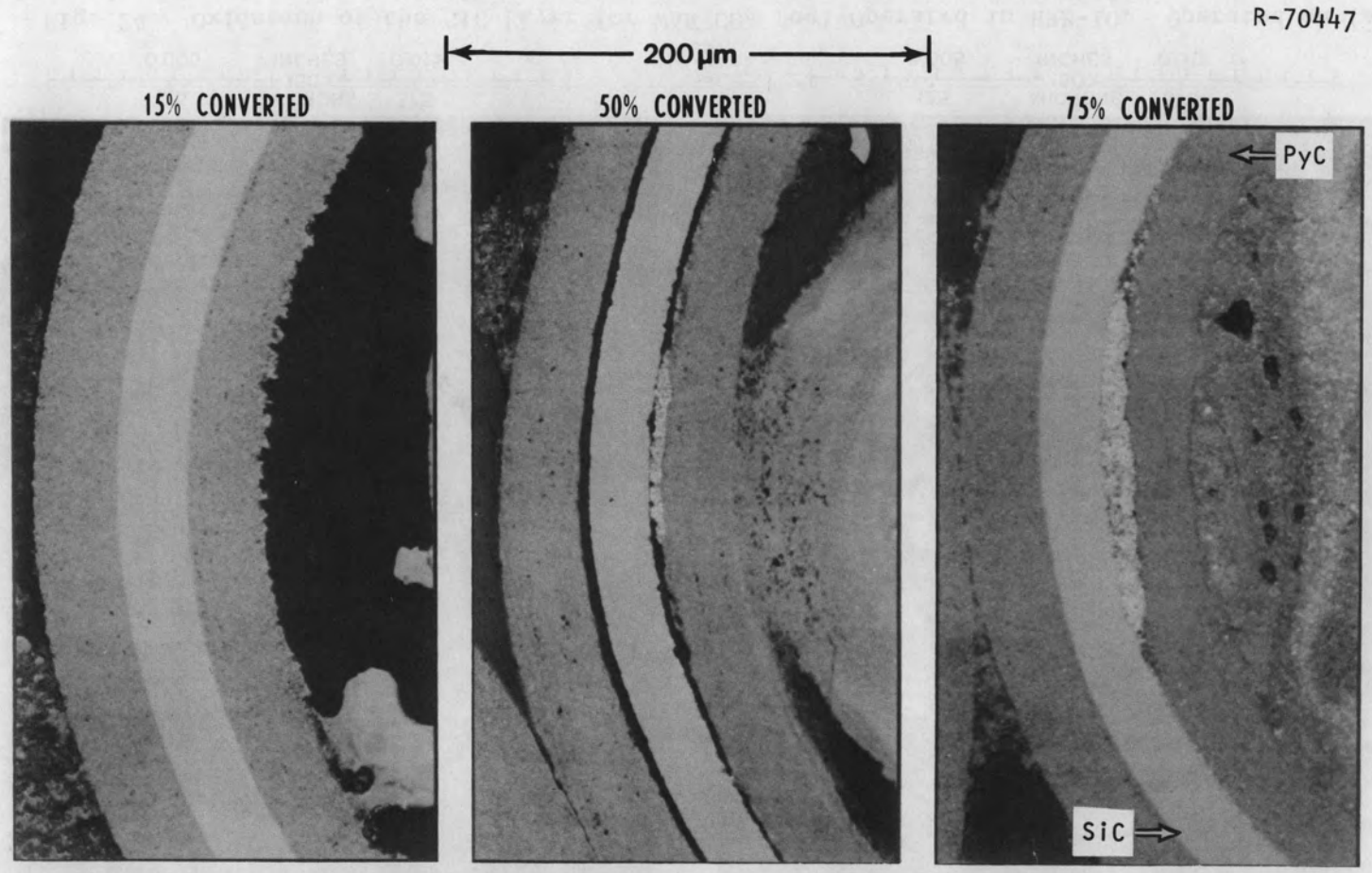

Fig. 23. Accumulation of Rare-Earth Fission Products at the Silicon Carbide Inner Pyrolytic Carbon Interface on the cold side of Triso-Coated WAR Kernels. Note the absence of fission products in the coating of the 15%-converted kernel.

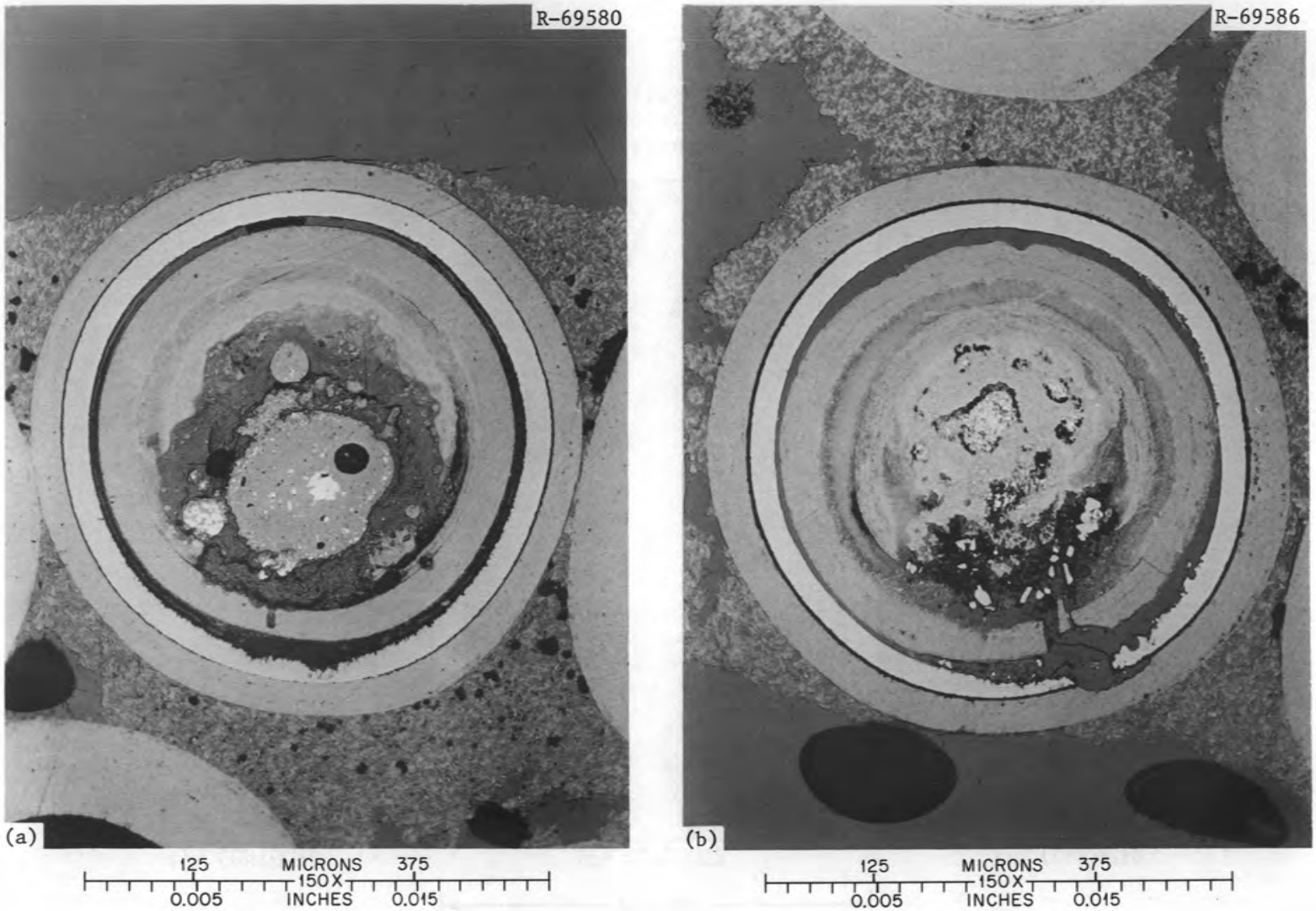

Fig. 24. Oxidation of the SiC Layer for WAR UO_2 Fuel Operated in HRB-10. Operated on (a) surface of fuel rod at about 1200°C and (b) center of fuel rod at about 1500°C.

By the current definition of failure developed for dense fissile kernels this fuel would be unacceptable; however, this definition of failure is not appropriate for WAR fuels. For fissile particles containing dense oxide kernels that are migrating up the temperature gradient, migration through the buffer layer means that the integrity of the pressure vessel has been compromised. Thus, failure is defined as migration through the buffer layer. However, for fissile particles containing WAR UO_2-UC_2 kernels with more than 15% carbide phase, temperature-gradient-dependent migration of the kernel has not been observed. The incorporation of the buffer layer into the kernel does not appear to influence the integrity of the outer coating layers. Irradiation testing is in progress to determine if the 15%-converted WAR fuel meets the performance criteria for fissile particles (less tha 0.7% failure during irradiation to full large HTGR exposure). Quantitative electron microprobe results have shown that the 15%-converted kernels retain all but about 12% of the rare-earth fission products that form during irradiation. Quantitative work is in progress for kernels of 50 and 75% conversion; from the optical comparisons that have already been made, we believe that these fuels will release more fission products than the 15%-converted fuel.

THERMODYNAMIC ANALYSIS

The previous section emphasized the importance of fission product attack of the inner low-temperature isotropic and silicon carbide layers, and the qualitative relationship between the amount of UO_2 phase present in the WAR kernel and the extent of attack observed. For processing it is desirable to maximize the amount of UO_2 present. Also, the manufacturer would like to have as much latitude as possible on the compositional requirements. Irradiation testing has suggested that WAR fuel between 15 and 75% converted from oxide to carbide will perform successfully, although there is some concern over the extent of fission product attack observed for the 75%-converted fuel. Thermodynamic analysis of the chemical system present in WAR fissile kernels suggests a lower limit of 15% conversion and an upper limit of about 70%.

The thermodynamic explanation of the observed irradiation phenomena is based on the chemical potential of oxygen (μ_{O_2}) for the fuel and fission-product equilibria. Here μ_{O_2} is defined as $RT \ln P_{O_2}$, in which R = 8.314 J mole^{-1} K^{-1} (1.987 cal mole^{-1} K^{-1}), T is temperature in K, and P_{O_2} is in atmospheres, with P_{O_2} in the standard state at 1 atm (1 atm = 0.1013 MPa).

The μ_{O_2} values have been calculated as a function of temperature for the probable oxide-carbide equilibria for uranium and each fission product. Typical equilibria are $UO_2 + 1.86C \rightarrow UC_{1.86} + O_2$, $2SrO + 4C \rightarrow 2SrC_2 + O_2$, and $1.33LaO_{1.5} + 2.66C \rightarrow 1.33LaC_2 + O_2$. Activity effects resulting from solution of fission-product oxides (primarily in UO_2)

were not considered because quantitative activity data are not available. The results of these calculations are given in Fig. 25; the SiO_2-C-SiC-O_2 equilibrium is also shown because of the silicon carbide presence in Triso coatings. The μ_{O_2} values of the various equilibria below 800 K establishes the following ranking in terms of increasing stability of the oxide versus the carbide: Ba, Zr, Eu, Sr, U, Sm, La, Pr, Nd, Ce, and Y. In other words, as μ_{O_2} is made more negative, the first to form will be BaC_2 instead of BaO, followed by ZrC instead of ZrO, and so on.

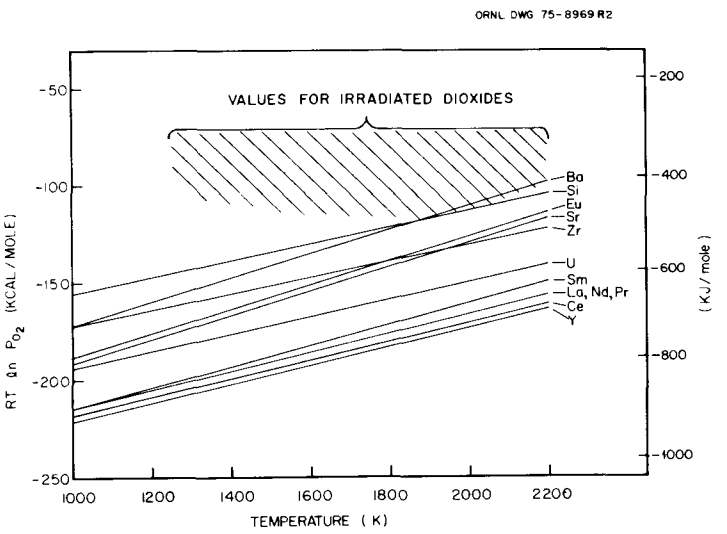

Fig. 25. Oxygen Potential vs Temperature for Various Oxide-Carbide Equilibria in the WAR UO_2-UC_2 System. Also shown are experimental UO_2 values for irradiated HTGR oxide fuels.

This report is concerned primarily with the effect of the UC_2-UO_2-C-O_2 equilibrium on the thermodynamics of the WAR HTGR fuel. As long as both UC_2 and UO_2 are present, then Fig. 25 demonstrates that Ba, Zr, Eu, Sr, and Si will be present as carbides, while Y, La, and all the rare-earth fission products except for europium will be present as oxides; europium is present as EuC_2. Another important effect of the UC_2-UO_2-C-O_2 equilibrium is the reaction of the UC_2 with oxygen that is released by the fissioning of $^{235}UO_2$ and that is not combined with oxide-forming fission products. At the μ_{O_2} of the UO_2-UC_2 system there is no interaction of the lanthanum, yttrium, or rare-earth sesquioxides $[(RE)O_{1.5}]$ with UO_2 that would increase the oxygen/uranium ratio above two.[21,22] Then the usual mass-balance calculations[23,24,25] demonstrate that each $^{235}UO_2$ fission leads to fission-product oxides that combine with only about 1.62 oxygen atoms even if one temporarily assumes that Ba, Zr, Eu, and Sr were to form oxides; this leaves 0.38 oxygen atom per fission that would combine with unfissioned UC_2 to form UO_2. It should also be noted that cesium and rubidium will not be present as oxides; the μ_{O_2} values of the UO_2-UC_2 system are much lower than those necessary for the stability of the uranates and molybdates of cesium and rubidium.[26]

Now consider a fuel particle at 75% FIMA in view of the above information and the fission-product yields for ^{235}U in a thermal flux.[27] For example, for the reaction (not an equilibrium) $2C + 2BaO + UC_2 \rightarrow UO_2 + 2BaC_2$, the initial amount of UC_2 required to maintain all barium as BaC_2 instead of BaO at 75% FIMA is (7.0% Ba/fission)(0.75 fission)(UC_2/2BaO) = 2.6% UC_2. Such calculations lead to the UC_2 requirements shown in Table 4. Thus, for an initial UC_2 content of $39.9 < UC_2 < 16.9$ in the UO_2-UC_2 kernel, at 75% FIMA no UC_2 would be present, barium would be present as BaC_2 and zirconium would be present as ZrO_2 and ZrC. All other fission products listed in Table 4 would be present as oxides along with the residual 25% UO_2 that did not fission.

Table 4. Calculated Initial UC_2 Amounts for Indicated Results at 75% FIMA

Purpose of UC_2 Addition	Initial UC_2 Required, %	
	For Each	Cumulative
UO_2 instead of high P_{CO}	14.3	14.3
BaC_2 instead of BaO	2.6	16.9
ZrC instead of ZrO_2	23	39.9
EuC_2 instead of $EuO_{1.5}$	0.4	40.3
SrC_2 instead of SrO	3.3	43.6
UC_2 instead of UO_2	25	68.6
SmC_2 instead of $SmO_{1.5}$	1.7	70.3
$(La,Nd,Pr)C_2$ instead of $(La,Nd,Pr)O_{1.5}$	18	88.3
CeC_2 instead of $CeO_{1.5}$	9.2	97.5
YC_2 instead of $YO_{1.5}$	2.3	99.8 (~100%)

It is important to note that the phases present depend on the extent of burnup as well as on the initial UC_2 content (Fig. 26). The results at an initial 20% UC_2 content exemplify this relationship. Both UC_2 and UO_2 are initially present, and these phases establish the μ_{O_2} up to about 34% FIMA. Fission-product systems at the more negative μ_{O_2} values (Fig. 25) are oxides, while those at more positive values are carbides. During fission to 34% FIMA, the UC_2 content is decreasing because it is reacting with oxygen that is released by the fissioning of the UO_2; this released oxygen would otherwise form ZrO_2, SrO, BaO, and $EuO_{1.5}$, as well as 0.38 CO per fission. Once burnup exceeds about 34% FIMA, UC_2 has disappeared and the next oxide-carbide equilibrium, SrO-SrC_2-C-O_2, establishes the μ_{O_2} for the system up to about 38% FIMA.

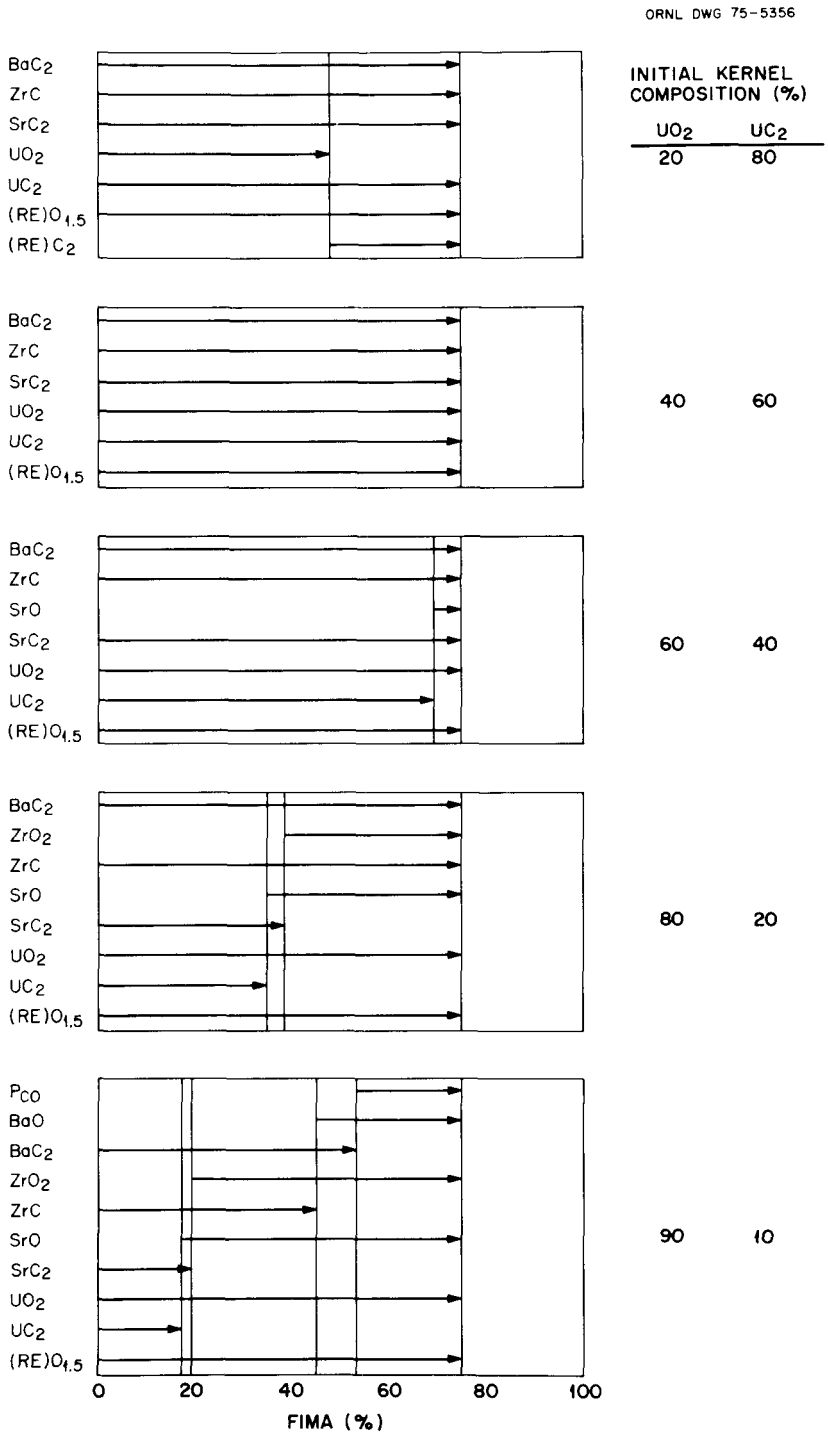

Fig. 26. Phases Present in a Fully Enriched UO_2-UC_2 Kernel as a Function of ^{235}U Burnup and Initial UC_2 Content. The $EuO_{1.5}$-EuC_2 system is not shown because it has a small (<1%) yield. However, its chemical behavior is different from the other lanthanides and it converts from the carbide to the oxide at about the same burnup as does the strontium.

The SrC_2 is completely converted to SrO at about 38% FIMA. After the trace of EuC_2 is converted to $EuO_{1.5}$ the ZrO_2-ZrC-C-O_2 equilibrium is then established and maintained to 75% FIMA.

Consideration of the data in Table 4 and Fig. 25 leads to a thermodynamic rationalization of the observed rare-earth behavior in the WAR UO_2-UC_2 fuel system. As long as the initial UC_2 percentage is less than 68.6%, all rare-earth elements (RE) except europium will be present as sesquioxides. These oxides remain in the kernel as illustrated above. When the initial UC_2 percentage exceeds 68.6%, then the rare-earth elements form dicarbides and the highest possible pressures of rare-earth neutral gases (P_{RE}); the presence of these dicarbides and P_{RE} are apparently associated with the silicon carbide interactions described earlier. The decreasing amount of rare-earth elements (RE) at the silicon carbide interface with the initial UO_2 amount of more than 68.6% may result from the equilibrium

$$(RE)O_{1.5} \rightarrow (RE)_g + 0.75\ O_2\ .$$

As the UO_2 content is increased, the μ_{O_2} and thus the P_{O_2} is increased, with a decrease in P_{RE}.

Initial UC_2 contents from 14.3 to 68.6% are apparently acceptable since no silicon carbide-degrading reactions have yet been observed in the irradiations.

Other potentially damaging effects occur for initial UC_2 percentages below 14.3%. The fission-released oxygen — as much as the 0.38 oxygen atom per fission mentioned earlier — reacts with a minor amount of the carbon in the particle to form carbon monoxide. [The carbon monoxide amounts are equivalent to the maximum of 0.31 (Kr + Xe) per ^{235}U fission.] If the inner LTI layer fails, the carbon monoxide will react with silicon carbide to form SiO_2, maintain the carbon monoxide pressure at that for the SiC-SiO_2-C-CO equilibrium (Fig. 25) and lead to failure of the silicon carbide layer. Thus, from thermodynamic considerations, the 14.3% initial UC_2 addition appears to be the minimum desirable amount.

DISCUSSION AND SUMMARY

Two important fuel failure mechanisms have been identified and appear to be directly related to fuel kernel chemical composition. These mechanisms are thermal migration (amoeba) of the fuel kernels up the temperature gradient and through the coatings and chemical interaction of fission products with the silicon carbide layer of Triso particles. Amoeba, which is a severe problem with dense oxide kernels, has not been a performance limiting problem with carbide fuels

in the temperature and temperature gradient regions of interest for the HTGR. Amoeba has not been observed in the WAR fuels containing more than 15% UC_2 in UO_2. Also, chemical interaction, a severe problem for dense carbide fuels, has been controlled in WAR fuels by controlling their composition.

Thermodynamic considerations suggest that kernel compositions ranging from 15 to 70% conversion from oxide to carbide should perform well. In kernels with less than 15% carbide the fission released oxygen will react with carbon to form carbon monoxide, which will raise the internal gas pressure and perhaps contribute to thermal migration. Should the carbon monoxide reach the silicon carbide layer, because of the failure of the inner LTI or because of a permeable inner LTI, the carbon monoxide will react with the silicon carbide to form SiO_2, and ultimately cause the silicon carbide layer to fail. In kernels with more than 70% carbide, insufficient oxygen is present to oxidize and thus stabilize the chemically active rare earth fission products, which will distill out of the kernel as carbides and attack the silicon carbide and inner LTI layers. Irradiation testing to date supports the conclusions of the thermodynamic studies. Compositions of 0, 15, 50, 75, and 100% carbide (the remainder oxide) have been tested. The WAR UO_2 fuel exhibited excessive thermal migration. The WAR UC_2 fuel exhibited excessive fission product attack of the silicon carbide layer, causing a high failure fraction in these particles. The 15, 50, and 75% carbide kernels performed well with increasing fission product attack of the silicon carbide evident with increasing carbide content.

The kernel process development work done so far indicates that the flexibility expected of WAR fuel, with repsect to kernel density and composition, is indeed possible in laboratory-scale equipment. The technology appears to be capable of extrapolation to production-scale equipment with no difficulty. Additional work on process development will continue to determine process latitudes.

The importance of this work is that a fissile fuel has been developed suitable for any HTGR application currently under consideration, up to irradiation temperatures of 1400°C. Probably, additional irradiation testing of optimum compositions will push this temperature limit still higher. Further, the processes required to produce these particles are readily adaptable to remote operation, which is essential for a recycle fuel. Direct comparisons of the WAR fuel with the current reference fresh fuel (dense UC_2) suggest superior performance by the WAR fuel, which further suggests that the WAR fuel could eventually become the reference fresh fissile fuel as well as the reference recycle fuel.

Future work should be directed at optimizing the WAR particle design and developing a product specification for manufacture. The fuel rod and fuel element designs need improvement to take advantage of the performance capabilities of the coated particles. Design modifications

that minimize the temperature difference between kernels and coolant will permit higher coolant temperatures and higher thermal efficiency to permit the HTGR to satisfy the needs for steam-cycle power production and process heat applications.

ACKNOWLEDGMENTS

The authors wish to acknowledge the contributions of many people in the areas of planning, execution, and evaluation of the numerous irradiation experiments that have been cited in this report. In particular, the authors wish to acknowledge W. P. Eatherly of the Metals and Ceramics Division and B. H. Montgomery of the Engineering Technology Division for their participation in the planning and design of the experiments; R. L. Hamner, J M Robbins, W. J. Lackey, G. W. Weber, W. H. Miller, Jr., C. Hamby, D. E. Rosson, J. B. Flynn, M. D. Allen, and C. E. DeVore of the Metals and Ceramics Division for fabrication and characterization of the fuel specimens; and H. T. Kerr of the Engineering Technology Division and R. L. Shepard of the Instrumentation and Controls Division for dosimetry and instrumentation, respectively. Postirradiation examination was conducted by E. L. Ryan, N. M. Atchley, L. G. Shrader, and T. J. Henson of the Metals and Ceramics Division. The authors also acknowledge the assistance of G. W. Griffith for technical editing and Julia Bishop for typing and makeup of the manuscript. We are particularly indebted to G. W. Weber and A. R. Olsen for their excellent technical reviews and many helpful comments.

REFERENCES

1. B. H. Montgomery, J M Robbins, and R. L. Hamner, "Irradiation Tests in HFIR Removable Beryllium Facility," *Gas-Cooled Reactor Programs Annu. Prog. Rep. Dec. 31, 1973*, ORNL-4975, pp. 89–127.

2. Preliminary Safety Analysis Report for Fulton Generating Station, Chapter 4.

3. T. B. Lindemer and R. L. Pearson, *Kernel Migration for HTGR Fuels from the Th-U-C-O-N System*, ORNL/TM-5207 (April 1976).

4. O. M. Stansfield, C. B. Scott, and J. Chin, "Kernel Migration in Coated Carbide Fuel Particles," *Nucl. Technol.* 25: 517–30 (1975).

5. Oak Ridge National Laboratory and Gulf General Atomic, *National HTGR Fuel Recycle Development Program Plan*, ORNL-4702 (August 1971) p. 16.

6. J. L. Scott et al., *An Irradiation Test of Bonded HTGR Coated Particle Fuels in an Instrumented Capsule in HFIR*, ORNL-TM-3460 (March 1972).

7. R. A. Olstad et al., *An Irradiation Test of Candidate HTGR Recycle Fuels in the H-1 and H-2 Capsules,* ORNL-TM-4397 (July 1974, Addendum April 1975).

8. K. H. Valentine et al., *Irradiation Performance of HTGR Fuel Rods in HFIR Experiments HRB-7 and -8,* report in preparation.

9. F. E. Clark, "Ion Exchange Resin Fuel Beads," *Nerva Fuel Element Dev. Prog. Sum. Rep. July 1966–June 1972,* Y-1852 (1973) part 5.

10. M. D. Silverman and C. B. Pollock, "Resin Fuel Particles for High-Temperature Gas-Cooled Reactors," pp. 245–46 in *11th Bienn. Conf. Carbon, Gatlinburg, Tenn., June 4–6, 1973,* CONF. 730601.

11. P. A. Haas, *HTGR Fuel Development: Use of UO_3 to Load Cation Exchange Resin for Microsphere Preparation,* ORNL-TM-3817 (1972).

12. K. J. Notz et al., *Bull. Am. Ceram. Soc.* 53(8): 621 (1974).

13. R. L. Beatty (abstract), *Bull. Am. Ceram. Soc.* 53(4): 363 (1974).

14. R. L. Beatty and E. L. Long, Jr., "Preparation and Performance of Coated Particle Nuclear Fuels Having UC_xO_y Kernels," pp. 315–16 in *12th Bienn. Conf. Carbon Extended Abstracts and Program,* July 28–August 1, 1975, Pittsburgh, Pennsylvania. Cosponsored by the American Carbon Society and the School of Engineering, University of Pittsburgh.

15. T. B. Lindemer, "Rate-Controlling Factors in the Carbothermic Synthesis of Advanced Fuels," *Nucl. Appl. Technol.* 9(5): 711–15 (November 1970).

16. F. J. Homan et al., *Irradiation Performance of HTGR Fuel Rods in HFIR Experiments HRB-4 and -5,* ORNL-5115 (June 1976).

17. K. H. Valentine et al., *Irradiation Performance of HTGR Fuel Rods in HFIR Experiments HRB-7 and -8,* report in preparation.

18. F. J. Homan et al., *Irradiation Performance of HTGR Fuel Rods in HFIR Experiments HRB-9 and -10,* report in preparation.

19. E. L. Long, Jr., et al, *Fabrication of ORNL Fuel Irradiated in the Peach Bottom Reactor and Postirradiation Examination of Recycle Test Elements 7 and 4,* ORNL-TM-4477 (September 1974).

20. R. A. Bradley et al., "Fuel Stick Fabrication," *Gas-Cooled Reactor and Thorium Utilization Programs Annu. Prog. Rep. Sept. 30, 1971,* ORNL-4760, pp. 52–55.

21. T. L. Markin and E. C. Crouch, "Thermodynamic Data for U-Ce Oxides," *J. Inorg. Nucl. Chem.* 32: 77–82 (1970).

22. J. F. Wadier, *Phase Diagram and Thermodynamic Properties of the Uranium-Neodymium-Oxygen System*, CEA-R-4507 (November 1973), p. 59.

23. R. H. Flowers and G. W. Horsley, *The Influence of Oxide Kernels on the Manufacture and Performance of Coated Particle Fuel*, AERE-R5949, (1968).

24. J. M. Leitnaker, "Applications of Thermodynamics for Predicting and Understanding the Performance of Fast Breeder Reactor Oxide Fuels," *J. Nucl. Mater.* 51: 95–105 (1974).

25. T. B. Lindemer and H. J. de Nordwall, *An Analysis of Chemical Failure of Coated UO_2 and Other Oxide Fuels in the High-Temperature Gas-Cooled Reactor*, ORNL-4926 (1974).

26. M. J. Kania et al., *Irradiation Performance of HTGR Fertile Fuel in HFIR Target Capsules HT-12 to 15: Part I — Experiment Description and Fission Product Behavior*, ORNL/TM-5305 (in press).

27. M. E. Meek and B. F. Rider, *Compilation of Fission Product Yields*, NEDO-12154 (1972).

ORNL/TM-5602
Distribution
Category UC-77

INTERNAL DISTRIBUTION

1–3. Central Research Library
4. Document Reference Section
5–14. Laboratory Records Department
15. Laboratory Records, ORNL RC
16. ORNL Patent Office
17. R. L. Beatty
18. R. A. Bradley
19. A. J. Caputo
20. J. A. Conlin
21. J. H. Coobs
22. D. Costanzo
23. F. L. Culler
24. W. P. Eatherly
25. R. B. Evans III
26. R. L. Hamner
27. R. F. Hibbs
28–30. M. R. Hill
31–34. F. J. Homan
35. D. R. Johnson
36. M. J. Kania
37–38. P. R. Kasten
39. H. T. Kerr
40. W. J. Lackey
41. T. B. Lindemer
42–44. E. L. Long, Jr.
45. R. K. Kibbe
46. A. L. Lotts
47. C. S. Morgan
48. M. T. Morgan
49. K. J. Notz
50. R. L. Pearson
51. W. H. Pechin
52. H. Postma
53. J M Robbins
54. R. L. Shepard
55. T. N. Tiegs
56. K. R. Thoms
57. J. R. Weir, Jr.

EXTERNAL DISTRIBUTION

58–65. ERDA DIVISION OF NUCLEAR FUEL CYCLE AND PRODUCTION, Washington, DC 20545

Director (2)
R. G. Bradley (1)
W. S. Schieb (5)

66–67. ERDA DIVISION OF REACTOR NUCLEAR RESEARCH AND APPLICATIONS, Washington, DC 20545

Director

68–69. ERDA IDAHO OPERATIONS OFFICE, P.O. Box 2108, Idaho Falls, ID 83401

C. E. Williams, Manager
Barry Smith

70. ERDA OFFICE OF PROGRAM MANAGEMENT, RESEARCH AND SPACE PROGRAMS, P.O. Box 81325, San Diego, CA 92138

J. B. Radcliffe

EXTERNAL DISTRIBUTION (Continued)

71. ERDA SAN FRANCISCO OPERATIONS OFFICE, 1333 Broadway, Wells Fargo Building, Oakland, CA 94612

R. D. Thorne, Manager

72–74. ERDA OAK RIDGE OPERATIONS OFFICE, P.O. Box E, Oak Ridge, TN 37830

Director, Research and Technical Support Division
Director, Reactor Division
F. E. Dearing, Reactor Division

75–245. ERDA TECHNICAL INFORMATION CENTER, P.O. Box 62, Oak Ridge, TN 37830

For distribution as shown in TID-4500 Distribution Category, UC-77 (Gas-Cooled Reactor Technology).

246–253. ERDA Exchange Agreements with Germany and Dragon Project.

☆ U.S. GOVERNMENT PRINTING OFFICE: 1976-748-189/90